© 2020. Published by The Company of Biologists Ltd | Journal of Cell Science (2020) 133, jcs248047. doi:10.1242/jcs.248047

RESEARCH ARTICLE

Microtubule polyglutamylation is important for regulating cytoskeletal architecture and motility in *Trypanosoma brucei*

Jana Jentzsch[1], Adal Sabri[2], Konstantin Speckner[2], Gertrud Lallinger-Kube[1], Matthias Weiss[2] and Klaus Ersfeld[1,*]

ABSTRACT

The shape of kinetoplastids, such as *Trypanosoma brucei*, is precisely defined during the stages of the life cycle and governed by a stable subpellicular microtubule cytoskeleton. During the cell cycle and transitions between life cycle stages, this stability has to transiently give way to a dynamic behaviour to enable cell division and morphological rearrangements. How these opposing requirements of the cytoskeleton are regulated is poorly understood. Two possible levels of regulation are activities of cytoskeleton-associated proteins and microtubule post-translational modifications (PTMs). Here, we investigate the functions of two putative tubulin polyglutamylases in *T. brucei*, TTLL6A and TTLL12B. Depletion of both proteins leads to a reduction in tubulin polyglutamylation *in situ* and is associated with disintegration of the posterior cell pole, loss of the microtubule plus-end-binding protein EB1 and alterations of microtubule dynamics. We also observe a reduced polyglutamylation of the flagellar axoneme. Quantitative motility analysis reveals that the PTM imbalance correlates with a transition from directional to diffusive cell movement. These data show that microtubule polyglutamylation has an important role in regulating cytoskeletal architecture and motility in the parasite *T. brucei*.

This article has an associated First Person interview with the first author of the paper.

KEY WORDS: Trypanosoma brucei, Cytoskeleton, Microtubules, Post-translational modifications

INTRODUCTION

A striking difference between the microtubule cytoskeletal architecture of many protists and metazoa are the structural constraints in the former group of organisms (Dawson and Paredez, 2013). In diverse protist phyla, including Apicomplexa (e.g. *Plasmodium* spp., *Toxoplasma* spp.), Euglenozoa (e.g. *Trypanosoma* spp., *Leishmania* spp.) or Fornicata (e.g. *Giardia* spp.), the microtubule cytoskeleton is characterised by highly ordered structures that are predetermined and by-and-large invariable for a given stage in the development of these organisms. Examples are the apical complex of *Plasmodium* and the subpellicular microtubule array of trypanosomes (Elmendorf et al., 2003; Hemphill et al., 1991; Morrissette and Sibley, 2002; Yubuki et al., 2016). This is in contrast to the highly dynamic and flexible arrangement of microtubules observed, for example, in a mammalian tissue culture cell. Yet, the primary sequences of tubulins are highly homologous and are not causative for such differences. Therefore, regulation of cytoskeletal architecture is very likely due to associated factors, such as organism-specific sets of microtubule-associated proteins and post-translational tubulin modifications.

The major determinant of shape and cellular integrity of trypanosomatids is the subpellicular microtubule cytoskeleton. It is arranged as an array of non-continuous, highly ordered parallel filaments of uniform polarity with the microtubule plus ends facing toward the posterior cell pole (Gull, 1999). Although the amino acid sequences of trypanosome α- and β-tubulins are highly homologous to their mammalian orthologues, the *in vivo* attributes of their respective microtubule cytoskeletons are very different. The subpellicular microtubule array of trypanosomes is extremely stable and is cold and detergent resistant (Robinson et al., 1991), in strong contrast to the microtubule cytoskeleton of the parasite's host. In addition to the subpellicular microtubule array, microtubules form the axoneme of the single flagellum of trypanosomes, responsible for motility of these parasites in their mammalian and insect hosts (Langousis and Hill, 2014). Using time-lapse microscopy and elaborate mathematical models, the intricate dynamics of the beating flagellum and the resulting swimming motion are by now well understood for wild-type trypanosomes (Alizadehrad et al., 2015; Uppaluri et al., 2012; Zaburdaev et al., 2011). Yet, effects due to changes in the regulation of the microtubule cytoskeleton have remained largely elusive.

Well-characterised regulators of microtubule dynamics in metazoa are the microtubule-associated proteins (MAPs) and a range of tubulin post-translational modifications (PTMs), such as reversible tyrosination, acetylation, phosphorylation, polyglycylation and polyglutamylation (Barra et al., 1973; Bodakuntla et al., 2019; Edde et al., 1990; Eipper, 1972; Raybin and Flavin, 1977; Redeker et al., 1994). With the exception of glycylation, typical microtubule PTMs have been detected in trypanosomes, either by using specific antibodies or mass spectrometric analysis (Sasse and Gull, 1988; Schneider et al., 1997; Woods et al., 1989). Based on sequence homology, genes coding for enzymes catalysing tubulin PTMs have been identified in the genomes of trypanosomatids. These include the tubulin–tyrosine ligase (TTL) and tubulin–tyrosine carboxypeptidase (vasohibin, also known as VASH), responsible for the tyrosination–detyrosination cycle of the C-terminal tyrosine of α-tubulin, and a family of enzymes collectively known as tubulin–tyrosine-ligase-like proteins (TTLLs). These enzymes are polyglutamylases and catalyse the addition of glutamate side chains of variable lengths to glutamate residues within the C-terminal tails of α- and β-tubulin. In

[1]Molecular Parasitology, Department of Biology, University of Bayreuth, Universitätsstr. 30, 95447 Bayreuth, Germany. [2]Experimental Physics I, Department of Physics, University of Bayreuth, Universitätsstr. 30, 95447 Bayreuth, Germany.

*Author for correspondence (klaus.ersfeld@uni-bayreuth.de)

G.L.-K., 0000-0001-8172-5238; K.E., 0000-0002-9995-8010

Handling Editor: Michael Way
Received 27 April 2020; Accepted 30 July 2020

Journal of Cell Science (2020) 133, jcs248047. doi:10.1242/jcs.248047

Trypanosoma brucei, nine TTLLs have been identified based on primary sequence analysis (Casanova et al., 2015; Janke et al., 2005).

Whereas many functional aspects of tubulin PTMs are well documented in mammalian cells and are associated with phenotypes such as axonal differentiation and transport, spermatogenesis and regulation of ciliar length, their significance for the unique structural organisation of the microtubule cytoskeleton or the flagellum of trypanosomes and related kinetoplastids is largely unexplored (Wloga et al., 2017). Only two recent studies have addressed the localisation and growth phenotypes of some members of the TTLL-family in *Leishmania major* and *Trypanosoma brucei* and functional aspects of vasohibin in *T. brucei*. Using RNA interference (RNAi), it was shown that only the depletion of one of the nine TTLL proteins (TTLL4B) is associated with growth arrest caused by blockage of cytokinesis (Basmaciyan et al., 2019; Casanova et al., 2015). It has also been shown that CRISPR-mediated knockout of vasohibin in *T. brucei* leads to morphological abnormalities and mitotic defects (van der Laan et al., 2019).

Inspired by these observations, we have performed an in-depth analysis of the putative polyglutamylases TTLL6A and TTLL12B in *T. brucei* procyclic forms. Using RNAi combined with biochemical analysis, immunofluorescence microscopy, electron microscopy and quantitative motility assays, we show that TTLL6A and TTLL12B depletion drastically perturbs cytoskeletal architecture. In particular, we observe a disintegration of the highly organised posterior end of the cell body into several lobes, which we term the 'glove' phenotype. Moreover, cells depleted of either TTLL6A or TTLL12B, even when not displaying the extreme 'glove' phenotype, exhibit a transition from a directional to a more diffusive motility, concomitant with a significant reduction of axonemal polyglutamylation.

RESULTS

TTLL6A and TTLL12B have *in vivo* polyglutamylase activities

The *T. brucei* proteins TTLL6A and TTLL12B belong to the family of tubulin–tyrosine-ligase-like proteins (Casanova et al., 2015) (see Table S1 for an overview). Except for the founding member of this family, tubulin–tyrosine ligase, all other members are either tubulin polyglutamylases or tubulin glycylases (van Dijk et al., 2007; Wloga et al., 2009). Based on sequence homology, *T. brucei* lacks the tubulin glycylase subfamily of TTLLs and, experimentally, no tubulin glycylation has been detected in trypanosomes (Schneider et al., 1997; Wloga et al., 2009). Hence, it is likely that all proteins of the TTLL family in *T. brucei* are polyglutamylases. Polyglutamylases are further subdivided into those enzymes initiating glutamylation, by adding a glutamine residue to a γ-carboxyl group of a single glutamate residue within the C-terminal tails of α- and β-tubulin, and elongating polyglutamylases, which then add further glutamyl residues to this initial branching glutamyl residue. In *T. brucei*, side chain lengths of up to 15 glutamyl residues on α-tubulin and up to six on β-tubulin have been described (Schneider et al., 1997). Enzymatic activities of some recombinant TTLLs of *L. major* have been assayed on mammalian tubulin and non-tubulin substrates; however, the specific properties of individual TTLL proteins in *T. brucei* are unknown (Casanova et al., 2015). To address this issue for the two proteins that are subjects of this study, we used the antibodies GT335 and PolyE to recognise different epitopes of polyglutamylated tubulin. The monoclonal antibody GT335 recognises polyglutamyl chains of any length and is therefore also suited to detect the initiating branching point, whereas the polyclonal antibody PolyE only binds to tubulins with glutamyl side chains longer than three glutamates (Shang et al., 2002; Wolff et al., 1992). Using RNAi, we depleted both TTLL proteins over a period of 2–3 d (Fig. S1), made cytoskeleton extracts and analysed this fraction using western blotting (Fig. 1). Knockdown of TTLL6A resulted in a reduction of total polyglutamylation levels by ∼50%, as measured by the GT335 signal, whereas the PolyE signal, indicative of chain elongation, was reduced by ∼20%. Equivalent experiments were carried out for TTLL12B. Here, the reduction in signal intensity was much stronger (an 80% reduction in GT335 signal, and a 70% reduction in PolyE signal). In contrast to observations of HeLa cell extracts, where GT335 detects multiple bands in addition to tubulin, and where a broad range of polyglutamylase substrates were identified (van Dijk et al., 2008), we did not observe such cross-reactivity in trypanosomes. Both for whole cell and cytoskeletal extracts, only tubulin was recognised (Fig. S2). Thus, at least at the detection level of chemiluminescent western blot analysis, no further major polyglutamylation substrates appear to exist in *T. brucei*.

Microtubule polyglutamylation is important for maintaining cytoskeletal integrity

Next, we analysed the morphology of cells that were subjected to RNAi-depletion of the two proteins (Fig. 2). After two days of RNAi induction of TTLL6A and TTLL12B, 34% (TTLL6A) and 22% (TTLL12B) of cells developed a highly distinctive phenotype. Cells grew much longer at the posterior end and displayed several lobular extensions that completely disrupted the normally highly organised pointed end of the cell (Fig. 2A,B). Whole-mount transmission electron microscopy (TEM) of cytoskeletons showed that the microtubules inside these lobes were continuous with the remaining cytoskeleton (Fig. 2D). The anterior end of the cells looked normal. Based on the glove-like appearance of these lobes we termed this morphology the 'glove' phenotype. Cells displaying this phenotype were on average 37 µm (TTLL12B) and 32 µm

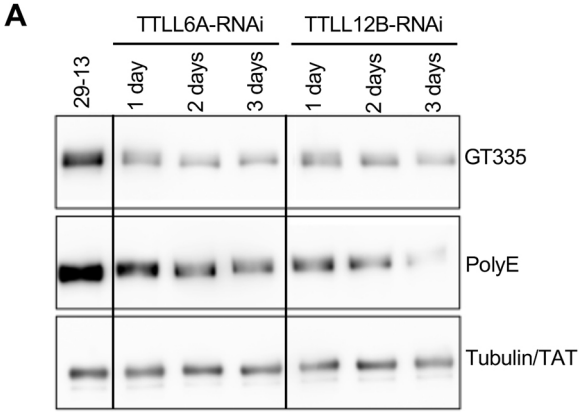

Fig. 1. Depletion of TTLL6A and TTLL12B reduces tubulin glutamylation. (A) Western blot analysis of cytoskeleton lysates from TTLL6A-RNAi and TTLL12B-RNAi cells induced over 3 d. 29-13 is the parental cell line and served as control. The GT335 antibody detects glutamyl side chains of any length, the PolyE antibody recognises polyglutamylation with at least four glutamate residues, the TAT antibody detects α-tubulin and serves as loading control. (B) The adjusted mean density values of the GT335 and PolyE signals of three independent western blots, normalised against the TAT loading control.

Journal of Cell Science (2020) 133, jcs248047. doi:10.1242/jcs.248047

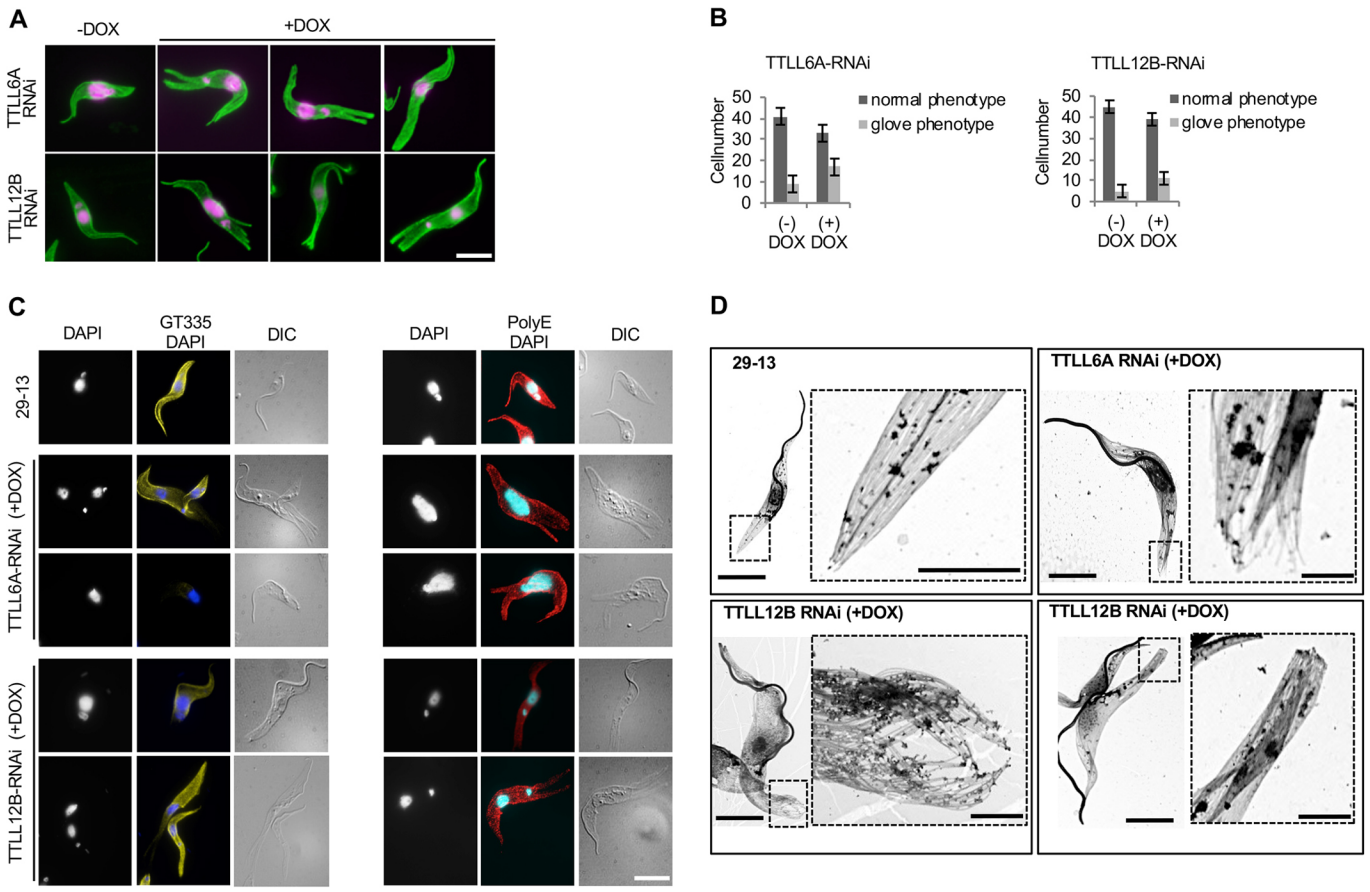

Fig. 2. Disruption of cellular architecture after TTLL6A and TTLL12B depletion. (A) Immunofluorescence images of non-induced (−DOX) cells and TTLL6A-RNAi or TTLL12B-RNAi cells induced for 2 d (+DOX). Cytoskeletons were stained using the TAT antibody to detect α-tubulin (green), nuclear and kinetoplast DNA was stained with DAPI (pink). (B) Statistical analysis of morphological phenotypes. Fifty cells of each cell line were counted in both non-induced (−DOX) and induced (+DOX) conditions for each of two experiments. Data are mean±s.d. (C) Immunofluorescence images of the parental cell line (29-13), TTLL6A- and TTLL12B-RNAi cells induced for 2 d (+DOX). Cytoskeletons were either stained with GT335 (yellow) or PolyE (red) antibodies, nuclear and kinetoplast DNA was stained with DAPI (blue). (D) TEM images of whole-mount cytoskeletons of wild-type cells (29-13) and cells after 2 d of depletion of TTLL6A (TTLL6A-RNAi) or TTLL12B (TTLL12B-RNAi). Boxed sections in the low magnification images are shown at higher magnifications in the large dashed boxes. Scale bars: 10 µm (A,C), 5 µm (D), 1 µm (D, enlargements).

(TTLL6A) in length, whereas the parental 29-13 cells were on average only 16 µm in length (Fig. S3).

In order to reveal a possible *in situ* correlation between aberrant microtubule glutamylation and altered cell morphology, we used GT335 and PolyE antibodies for immunofluorescence analysis of cytoskeletal preparations (Fig. 2C). In wild-type trypanosomes, cells were uniformly stained with either antibody. However, in cells depleted of TTLL6A, the GT335 antibody staining was strongly reduced. In particular, the lobes of 'glove' cells were almost devoid of staining. Using the PolyE antibody, we observed a signal reduction as well, but it appeared less pronounced and was distributed more uniformly across the cell body. Results using TTLL12B-depleted cells were similar, except that here the reduced staining intensity with PolyE was more evident across the cell body, and staining was almost completely absent towards the posterior tip and within the protrusions (Fig. 2C). These results were congruent with our western blot analysis.

Imbalanced polyglutamylation affects microtubule dynamics and recruitment of the end-binding protein EB1

We next asked whether aberrant polyglutamylation had an effect on microtubule dynamics. To address this, we stained cytoskeletal preparations with YL1/2, an antibody specific for tyrosinated α-tubulin (Kilmartin et al., 1982). Tyrosinated microtubules are a marker for newly assembled microtubules in many model systems, including *T. brucei* (Sherwin and Gull, 1989; Sherwin et al., 1987). In contrast to wild-type cells where, in addition to the normal basal body staining, only a faint staining at the posterior end was visible, TTLL6A- and TTLL12B-depleted cells displayed an extremely strong YL1/2 signal, which extended from the posterior tip of apparently morphologically intact cells or from the tips of the lobes in cells with a disrupted posterior pole towards the middle of the cell (Fig. 3A; Fig. S4). These results were consistent with western blot analysis of cytoskeletal extracts (Fig. 3B). After 1 d and 2 d of RNAi depletion of either TTLL protein the YL1/2 signal strongly increased.

To investigate this phenotype further, we analysed the distribution of the microtubule plus-end-binding protein EB1, using it as a marker for a correctly assembled and organised cell posterior tip structure (Fig. 3C). EB1 is one of the few conserved microtubule-binding proteins in *T. brucei*. In other organisms, EB1 has been shown to direct the dynamics of the plus end of microtubules by regulating microtubule growth and length and by serving as a platform to recruit other regulatory proteins (Nehlig et al., 2017). Genome-wide RNAi analysis by RIT-seq indicated a reduced fitness of *T. brucei* after EB1 depletion (Alsford et al.,

Journal of Cell Science (2020) 133, jcs248047. doi:10.1242/jcs.248047

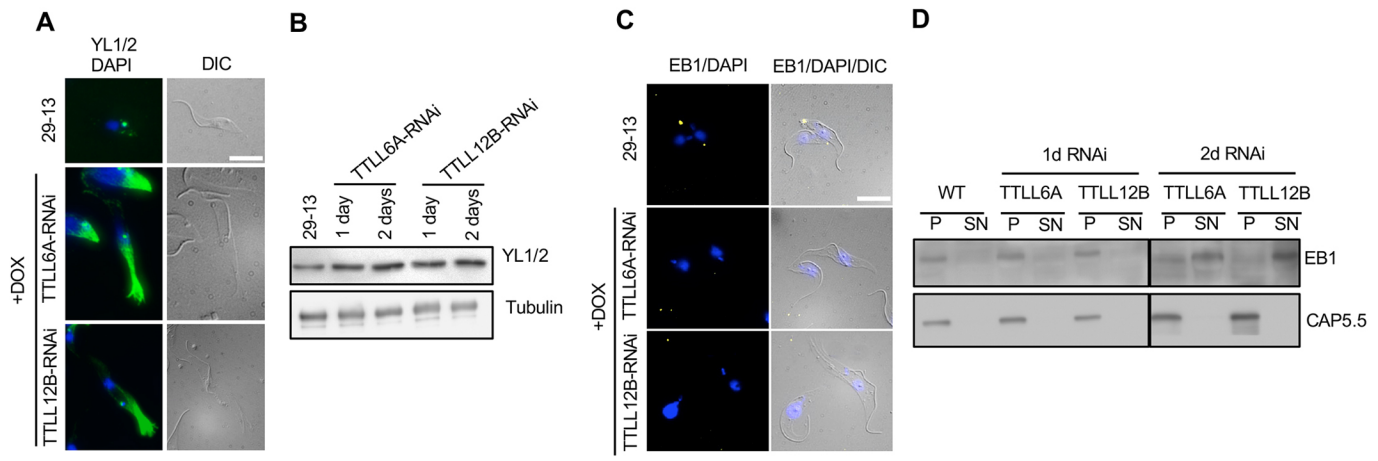

Fig. 3. Effect of TTLL6A and TTLL12B depletion on the distribution of tyrosinated microtubules and localisation of end-binding protein EB1. (A) Immunofluorescence images of cytoskeletons of wild-type cells (29-13) and RNAi cells (TTLL6A-RNAi, TTLL12B-RNAi) after 2 d induction. Tyrosinated α-tubulin was stained with YL1/2 (green), nuclear and kinetoplast DNA was stained with DAPI (blue). The single dot in each cell represents the basal body. (B) Western blot analysis of cytoskeleton lysates of wild-type cells (29-13) and RNAi cells after 1 d and 2 d of induction. Tyrosinated α-tubulin was detected with YL1/2, the TAT antibody (lower panel) detects α-tubulin and served as loading control. (C) Fluorescence images of wild-type cells (29-13) and RNAi cells induced for 2 d (+DOX). Depletion of TTLL6A or TTLL12B causes loss of the end-binding protein 1 (EB1), stained using a monoclonal anti-EB1 antibody (yellow). Nuclear and kinetoplast DNA was stained with DAPI (blue). (D) Western blot analysis of soluble (SN) and cytoskeletal (P) cell fractions probed with anti-EB1 antibody in wild-type cells (WT) and after 1 d and 2 d of TTLL6A and TTLL12B depletion. Anti-CAP5.5 antibody was used as a marker of the subpellicular cytoskeleton. Scale bars: 10 µm.

2011). We generated a monoclonal mouse antibody against *T. brucei* EB1. The single EB1 orthologue in *T. brucei* is, as expected and shown previously (Sheriff et al., 2014), localised to the posterior tip of the cell, where plus ends of many individual microtubules converge. In cells depleted of either TTLL6A or TTLL12B the EB1 signal was undetectable, both in cells that had developed the 'glove' phenotype and also in cells of apparently normal morphology. On a biochemical level, this was accompanied by a shift of the EB1 protein from the cytoskeleton fraction into the Triton X-100-soluble cell fraction (Fig. 3D). This not only substantiates the disrupted organisation of the cell tip at a molecular level, but also points to an important role for microtubule polyglutamylation in the recruitment of EB1. Because a canonical function of EB1 in other organisms is the regulation of microtubule length, we hypothesise that the failure of EB1 recruitment to the posterior tip might be a contributing factor to the loss of cytoskeletal organisation. However, in another study no such phenotype was reported after EB1 depletion by RNAi, but the level of EB1 knockdown was not determined (Sheriff et al., 2014).

Not surprisingly, the drastic effect of aberrant polyglutamylation on cell morphology also affects cytokinesis and cell growth (Fig. 4). After 2 d of depletion of either polyglutamylase, anucleate cells

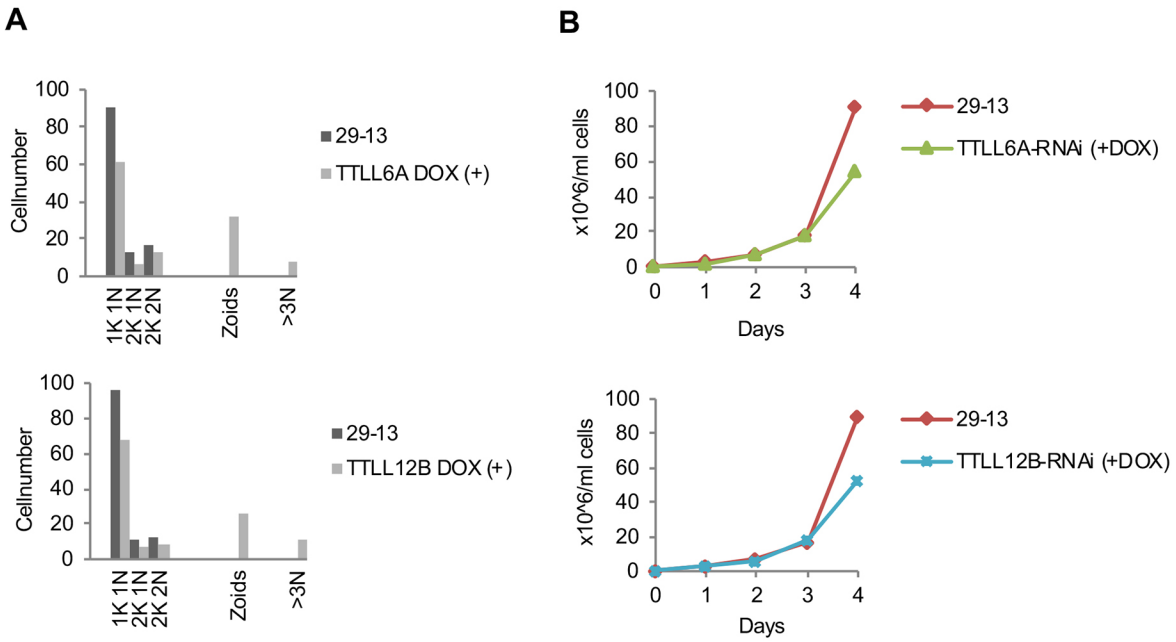

Fig. 4. Cytokinesis and growth defects after depletion of TTLL6A and TTLL12B. TTLL6A-RNAi and TTLL12B-RNAi cells were induced for 2 d (+DOX). (A) Distribution of the number of multinucleated cells and zoids in TTLL6A-RNAi and TTLL12B-RNAi cells. 29-13 is the parental cell line. K, kinetoplast; N, nucleus. *n*=120. (B) Cell growth of wild-type cells (29-13) and cells depleted of either TTLL6A or TTLL12B was measured over 4 d.

Journal of Cell Science (2020) 133, jcs248047. doi:10.1242/jcs.248047

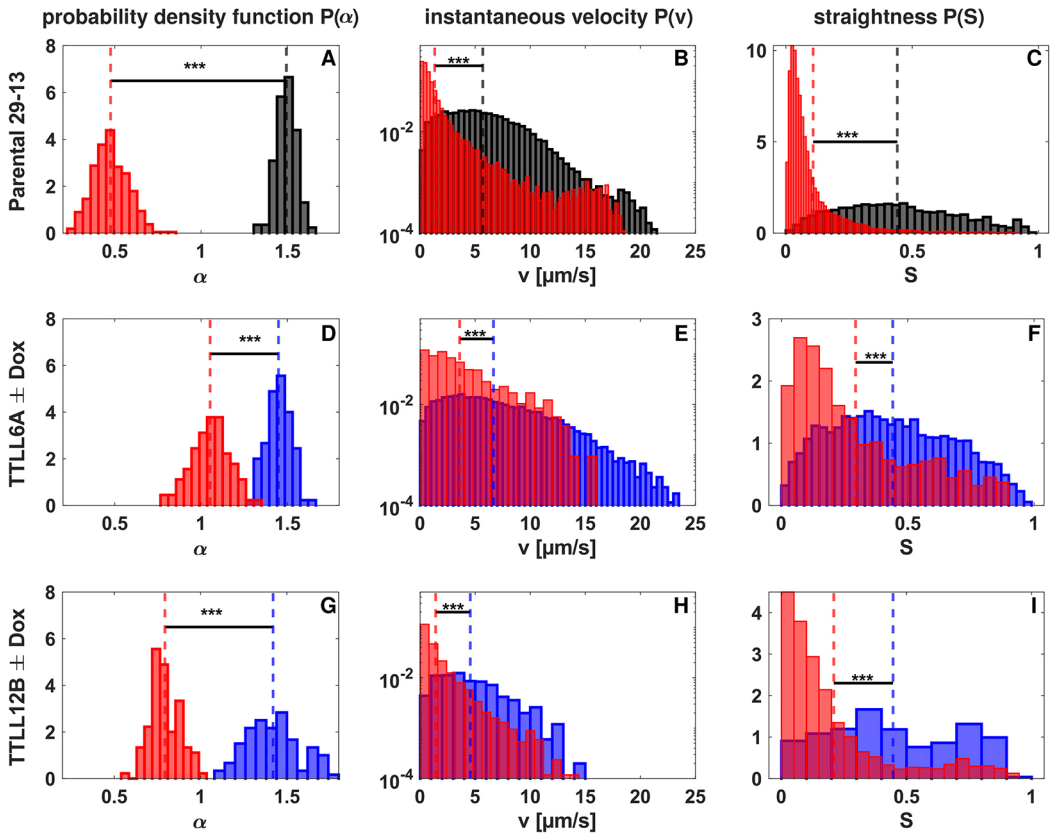

Fig. 5. Changes in cell motility after TTLL6A and TTLL12B depletion. Probability density functions of scaling exponents of trajectory mean square displacement, *P*(α) (left column); instantaneous velocity, *P*(v) (middle column); and trajectory straightness, *P*(S) (right column). Highly significant changes are seen for untreated trypanosomes (A–C) between the freely moving state (black histograms) and when restrained on lysine-coated coverslips (red histograms). RNAi treatment against TTLL6A (D–F) and TTLL12B (G–I) did not result in marked changes of *P*(α) without induction (blue histograms). Upon induction (red histograms), highly significant changes were observed. Similar changes were also seen for *P*(v) and *P*(*S*). Dashed vertical lines indicate the mean, as stated in Table 1. ***$P<0.001$ (two-sample Kolmogorov–Smirnov test).

('zoids') and cells with additional nuclei were readily detectable, and after 3 d of RNAi induction a population growth defect was evident.

Microtubule polyglutamylation deficiencies inhibit directional cell motility

Upon superficial visual inspection of cells after RNAi depletion of either polyglutamylase we noticed altered swimming behaviour. In order to probe the macroscopic impact of compromised post-translational modifications of microtubules in a quantitative manner, we tracked individual trypanosomes with bright-field microscopy under varying conditions (see Materials and Methods for details); representative tracks are shown in Fig. S5. To distinguish between aberrant swimming due to gross morphological distortions (glove phenotype cells) and more subtle defects, only cells with a normal morphological appearance were selected for motion analysis.

With the aim of revealing quantitative differences after depleting TTLL6A or TTLL12B, we first extracted for each of the recorded trajectories the scaling exponent α of the mean square displacement [see Eqn (1) in Materials and Methods] and combined all α values for trajectories at the same condition into a normalised histogram, *P*(α) [i.e. into a probability density function (PDF)]. These PDFs for all conditions are summarised in the left column of Fig. 5; corresponding mean values and standard deviations are given in Table 1. Datasets were tested for significant differences using a two-sample Kolmogorov–Smirnov test because the underlying PDFs were not Gaussian (as required for a Student's *t*-test).

For parental 29-13 procyclic trypanosomes (Fig. 5A, black bars), we observed a fairly narrow PDF around a mean $\langle\alpha\rangle\approx1.5$, indicating a clear super-diffusive mode of motion. This finding compares favourably to the expectation for microscopic swimmers with a run-and-tumble-like mode of motion, whereas (sub)diffusive or ballistic motion would have resulted in values of $\alpha\leq1$ or $\alpha=2$, respectively.

Table 1. Statistical details of the motility analysis

		Number of trajectories	⟨α⟩±s.d.(α)	⟨v⟩±s.d.(v) [μm/s]	⟨*S*⟩±s.d.(*S*)
Wild type	Free	187	1.49±0.06	5.70±3.46	0.44±0.23
	Lysine-coated	417	0.48±0.10	1.32±2.18	0.11±0.13
TTLL6A	Non-induced	352	1.45±0.07	6.66±4.40	0.44±0.24
	Induced	28	1.05±0.11	3.59±3.04	0.29±0.23
TTLL12B	Non-induced	15	1.42±0.15	4.55±2.85	0.45±0.25
	Induced	61	0.79±0.09	1.41±1.79	0.21±0.22

Journal of Cell Science (2020) 133, jcs248047. doi:10.1242/jcs.248047

In line with this notion, trypanosomes that had been attached to lysine-coated coverslips showed, as expected, a highly significant shift of $P(\alpha)$ to smaller values around a mean $\langle\alpha\rangle\approx0.5$ (Fig. 5A, red bars). Examining cells carrying RNAi constructs for TTLL6A and TTLL12B, without RNAi induction, only resulted in small changes of $P(\alpha)$ (Fig. 5D,G, blue bars). Yet, upon induction highly significant shifts to smaller α values were observed. Whereas RNAi against TTLL6A resulted in a motion pattern near to normal Brownian diffusion ($\alpha=1$), depletion of TTLL12B even featured a clear subdiffusive motion ($\langle\alpha\rangle\approx0.8$) (Fig. 5D,G, red bars). Thus, highly significant changes in the mode of motion are observed upon RNAi-mediated depletion of TTLL6A and TTLL12B.

As a second observable parameter, we extracted the instantaneous velocities for each position in all trajectories. To this end, we calculated the instantaneous velocities at each recorded position by taking the ratio of the displacement Δr taken within five frames [i.e. within a period of $\delta t=5\Delta t=0.5$ s (where Δt is the frame time)]. Again, we combined all velocities at the same condition into a single PDF, $P(v)$ (Fig. 5, middle column). As expected, a drastic change of $P(v)$ was seen for untreated trypanosomes when hindering their motion by attaching them to lysine-coated coverslips (Fig. 5B). The average velocity was decreased about fourfold (Table 1). As before, uninduced RNAi cells only showed mild changes, yet for induced cells the depletion of TTLL6A and TTLL12B resulted in highly significant changes of $P(v)$ and the associated mean (Fig. 5E,H). Similar to the findings for $P(\alpha)$, knocking down TTLL12B had a somewhat stronger effect (see mean values in Table 1). Thus, the instantaneous velocities also revealed a highly significant change in the mobility of trypanosomes upon knocking down either protein.

Finally, we also probed whether the directionality of motion of the trypanosomes changed upon treatment, because this aspect is not tested directly in the two previously discussed parameters. As a measure we used the straightness (S) of trajectories (defined in Eqn 2, Materials and Methods). As before, straightness values for the same condition were summarised in a PDF, $P(S)$, shown in the right column of Fig. 5. Whereas parental and freely moving trypanosomes displayed motion with large values of straightness and with high variation among trajectories, hindered motion on lysine-coated coverslips shifted $P(S)$ to markedly smaller values (Fig. 5C). Again, the change was found to be highly significant. In line with our aforementioned observations, uninduced RNAi treatment had little effect, whereas an induced depletion of TTLL6A or TTLL12B led to a highly significant reduction of the straightness values (Fig. 5F,I) (see also Table 1). Again, depletion of TTLL12B showed a stronger effect than depletion of TTLL6A. Thus, depletion of TTLL6A or TTLL12B not only reduced the average velocity but also led to less straight trajectories, that is, the RNAi treatment enhanced the occurrence of tumbling motion relative to the running phases of trypanosome motility.

Because it is difficult, using the methods outlined above, to assign this motility phenotype to a flagellar defect, we also measured helical frequency data of flagella (Fig. S6). The PDF of the helical frequency of trypanosome motion, $P(f)$, as determined from individual trajectories, showed a pronounced peak around $f=1$ Hz for the parental cell line (Fig. S6, black histogram). Here, the shape and width of the distribution not only encodes temporal and cell-dependent variation in the pattern of motion, but also reflects uncertainties in the evaluation protocol (see below). Whereas non-induced TTLL6A and TTLL12B strains (Fig. S6, blue histograms) show distributions that are almost congruent with the parental line, RNAi-induced cells (Fig. S6, red histograms) show a marked shift towards higher frequencies, supposedly reflecting a change in the action of the flagellum.

Flagellar glutamylation defects correlate with aberrant motility

Motility of trypanosomes is mediated by the flagellum. Compromised flagellar functionality is detrimental to many aspects of the *T. brucei* life cycle (Broadhead et al., 2006; Engstler et al., 2007; Robinson and Gull, 1991; Rotureau et al., 2014). To analyse a possible link between the altered swimming patterns after polyglutamylase depletion and underlying flagellar biology, we quantified axonemal polyglutamylation by immunofluorescence of whole cell cytoskeleton preparations and western blotting of isolated flagella (Fig. 6). The depletion of TTLL6A led to a significant reduction (of ∼30%) in flagellar fluorescence when probed with the GT335 antibody (recognising all polyglutamyl side chains) and a small decrease in labelling when probed only for long side chains using the PolyE antibody (Fig. 6A,B). Depletion of TTLL12B led to an even more pronounced reduction in the fluorescence intensity, highly significant for both antibodies used (a reduction of ∼70% for both GT335 and PolyE signals).

In addition, we probed western blots of extracts from isolated flagella with GT335 and PolyE antibodies (Fig. 6C). For flagella from both TTLL6A- and TTLL12B-RNAi cells, a strong reduction of the signal, indicating reduced polyglutamylation of axonemal microtubules, was detected. The reduction was stronger for the PolyE signal, suggesting primarily a reduction in long (>3) polyglutamyl chains. Contamination of the flagellar preparations with tubulin of the subpellicular cytoskeleton was minimal, because CAP5.5, a marker protein exclusively associated with the subpellicular cytoskeleton and absent from the flagellum, was not detectable in the axonemal fraction (Hertz-Fowler et al., 2001). The structural protein PFRA, which is restricted to the flagellum, was readily detectable in this fraction.

DISCUSSION

The shape of a trypanosome cell is crucially dependent on the subpellicular cytoskeleton, a highly ordered array of sub-plasma-membrane, parallel microtubules (Sinclair and de Graffenried, 2019). In contrast to the dynamic microtubule cytoskeleton in mammalian cells, the trypanosome microtubule corset is extremely stable. Yet, during defined stages of the cell and life cycle this stability has to give way to a transient dynamic nature, such as for the semiconservative duplication of the subpellicular microtubule array during cell duplication and for changes in morphology and microtubule-dependent organelle positioning during differentiation (Matthews et al., 1995; Robinson and Gull, 1991; Robinson et al., 1995; Sherwin and Gull, 1989). How such transitions between stability and dynamic changes are regulated is unknown. In mammalian systems, the regulation of microtubule dynamics is well characterised and it is essentially controlled at three levels: the biochemical properties of tubulins, including the expression of various isoforms; the activity of many microtubule-associated proteins (MAPs); and a variety of post-translational modifications of α- and β-tubulin (Westermann and Weber, 2003). The latter is also referred to as the tubulin code, in analogy to the histone code (Janke, 2014). *T. brucei* only has one α- and one β-tubulin variant, arranged as tandem repeats in the genome (Ersfeld et al., 1998; Thomashow et al., 1983). Therefore, regulation via differential isoform expression is not an option. Proteins associated with the subpellicular cytoskeleton have been identified in *T. brucei*, but their precise roles in microtubule stability and dynamics is not well

Journal of Cell Science (2020) 133, jcs248047. doi:10.1242/jcs.248047

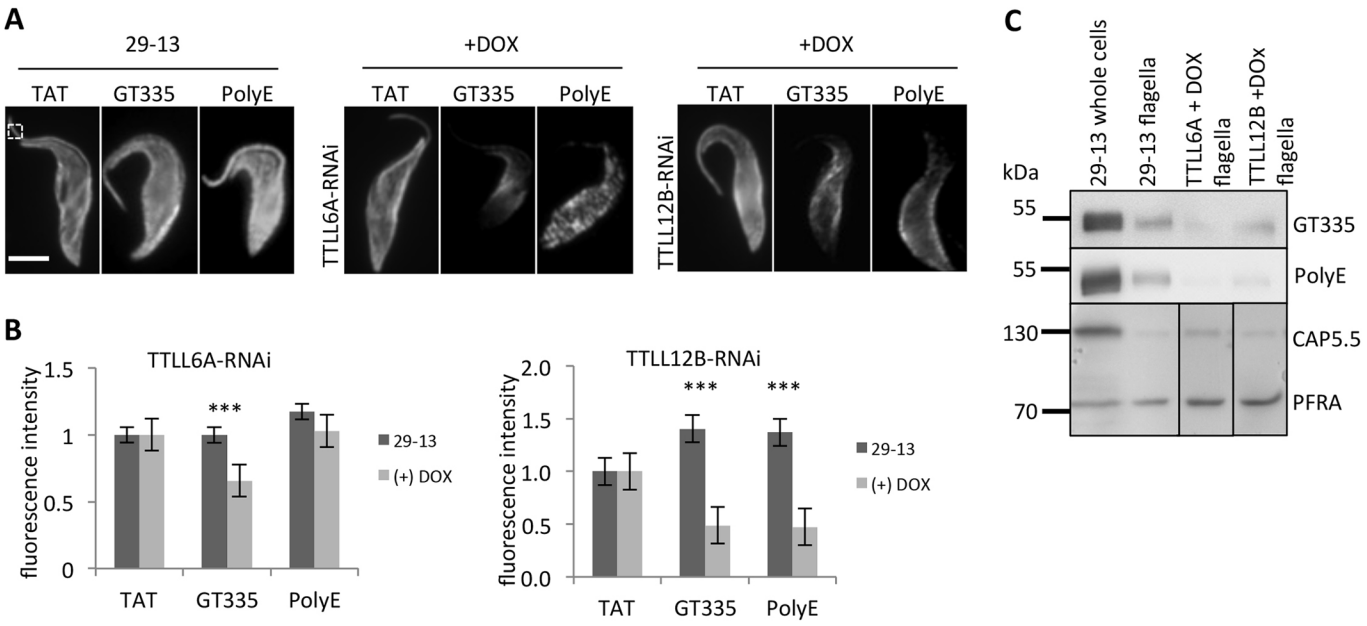

Fig. 6. Reduction of glutamylation of the axoneme after depletion of TTLL6A and TTLL12B. Depletion of either TTLL6A or TTLL12B for 2 d (+DOX) causes reduction of flagellar glutamylation, as observed by staining with GT335 or PolyE antibodies in immunofluorescence (A,B) and western blot (C). (A) The dotted square indicates the position of the fluorescence intensity measurements. The TAT antibody (α-tubulin) serves as a control. 29-13 is the parental cell line. Scale bar: 6 µm. (B) Quantification of mean±s.e.m. fluorescence intensity. n=16 for both induced (+DOX) and 29-13 cells. ***P<0.001; no asterisk, P>0.05 (t-test). (C) Western blots of whole cell lysates and flagella of 29-13 cells and flagella of TTLL6A-RNAi and TTLL12B-RNAi cells. CAP5.5 and PFRA antibodies serve as controls for flagellar enrichment and loading.

understood (Sinclair and de Graffenried, 2019). Some are essential for maintenance of morphology and cytokinesis (Baines and Gull, 2008; Olego-Fernandez et al., 2009; Vedrenne et al., 2002). Many enzymes involved in post-translational modifications of α- and β-tubulin are conserved between a wide range of organisms, including trypanosomes. The largest group of these proteins is the family of tubulin–tyrosine-ligase-like (TTLL) enzymes (Janke et al., 2005). They are named due to a shared sequence domain that is present in the founding member of this family, the tubulin–tyrosine ligase (Dideberg and Bertrand, 1998; Ersfeld et al., 1993). Whereas this enzyme catalyses the addition of tyrosine to the C terminus of α-tubulin as part of the detyrosination–tyrosination cycle, the other members are either polyglycylases or polyglutamylases, catalysing the addition of glycine or glutamate side chains to α- and β-tubulin (Janke, 2014).

Here, we have analysed two proteins of the TTLL family, TTLL6A and TTLL12B. The nomenclature is based on the phylogenetic classification of this family by Janke et al. (2005) and van Dijk et al. (2007), which was subsequently applied to kinetoplastids by Casanova et al. (2015). TTLL6-group proteins have, *in vitro* and *in vivo*, been identified as polyglutamylases, based on their ability to increase microtubule polyglutamylation levels in cultured HeLa cells (van Dijk et al., 2007). In this model, TTLL12 has shown negligible activity. Although the protein sequence of the TTLL12 group, including *T. brucei* TTLL12B, has a (relatively poorly conserved) canonical TTL domain, it lacks, at sequence alignment level, the so-called extended TTL domain, which is characteristic of most other TTLL proteins. However, our analysis clearly showed that depletion of TTLL12B by RNAi leads to a decrease in tubulin polyglutamylation, both *in situ* and by western blot analysis. In particular, the reactivity of both α- and β-tubulin with the antibody GT335, which recognises polyglutamate side chains of any length, was strongly decreased. The depletion of TTLL6A also resulted in a decrease in signal, both for GT335 and for PolyE (which recognises side chains longer than three glutamate residues). In a previous study, using HeLa and mouse brain tubulin as substrate, TTLL6A from the kinetoplastid *L. major* was found to show a moderate glutamylase activity *in vitro*. TTLL12B was not analysed in that study (Casanova et al., 2015). To summarise, both TTLL6A and TTLL12B have been identified as genuine tubulin polyglutamylases in *T. brucei*.

Numerous studies in recent years have shown the involvement of tubulin PTMs in many functional attributes of microtubule biology. Imbalanced PTMs are associated with a number of human diseases, particularly affecting highly ordered microtubule structures such as cilia, flagella and neurons (Magiera et al., 2018). Many aspects of the cell morphology of trypanosomes are equally defined by two highly ordered microtubule structures, the subpellicular cytoskeleton and the axoneme of the flagellum. Given the conservation of many tubulin PTMs in trypanosomes, it is reasonable to assume that they play a significant role regulating the functionality of these microtubule structures and, moreover, provide an excellent model to study tubulin PTMs in this experimentally highly accessible organism.

The depletion of either TTLL6A or TTLL12B resulted in a phenotype of a drastically altered cell morphology caused by an abnormal organisation of the subpellicular microtubules. The posterior end of a trypanosome cell normally terminates with a pointed end where ∼30–40 microtubule filaments converge, with their plus ends arranged into an ‘open-pipe’-like structure (Hemphill et al., 1991). In ∼30% of TTLL-depleted cells, this organisation was disrupted, and instead the cells outgrew at the tip to form a blunt end, or the outgrowing end branched into several protrusions that could form further sub-branches during elongation. Interestingly, the anterior end was, as observed using light microscopy, unaffected. An outgrowth of microtubules at the posterior tip of *T. brucei* has been described several times in connection with analysis of proteins important for cell cycle progression and life cycle differentiation and was termed the ‘nozzle’ phenotype (Hammarton et al., 2004;

Journal of Cell Science (2020) 133, jcs248047. doi:10.1242/jcs.248047

Hendriks et al., 2001; Pasternack et al., 2015). However, the pointed single end was always maintained in these cells, indicating a generally intact microtubule organisation but defects in the timing of cell cycle progression and coordination. The cause of the phenotype in TTLL-depleted cells is different, because the fundamental organisation of microtubules is lost. This is reinforced by the following two observations. First, the strong contrast in levels of tyrosinated microtubules, as revealed by YL1/2 staining between the parental cell line and the glutamylase-depleted cells, indicates a major imbalance in the dynamics of microtubule assembly. Second, the microtubule plus-end-binding protein EB1 homologue is no longer detectable at the posterior tip of the cell upon TTLL depletion and separates into the detergent soluble cell fraction rather than, as in wild-type cells, the cytoskeleton fraction. The loss of EB1 is reminiscent of observations made in mammalian neuronal cells and yeast that the localisation of CAP-Gly-motif-containing microtubule end-binding proteins, such as Bik1p in yeast, CLIP170 (also known as CLIP1) and p150Glued (DCTN1), is lost after abolishing the post-translational tyrosination of α-tubulin or generating a yeast mutant lacking the C-terminal phenylalanine of α-tubulin (Badin-Larcon et al., 2004; Erck et al., 2005; Peris et al., 2006). The molecular basis of this observation is that CAP-Gly proteins require a composite binding site, consisting of tyrosinated α-tubulin and the presence of EB1 (Bieling et al., 2008). EB1 localisation was not affected by the tyrosination defect and, to our knowledge, the effect of polyglutamylation on EB1 localisation has not been addressed so far. However, using molecular simulations, it was recently shown that polyglutamylation might affect diffusion rates of EB1 along microtubule filaments (Bigman and Levy, 2020). We hypothesise that a regulated polyglutamylation, like tyrosination–detyrosination, is required as a platform for the recruitment of a specific subset of microtubule-associated proteins. EB1 proteins are considered as master regulators of the so-called +TIP network, an assembly of plus-end microtubule proteins essential for microtubule assembly and dynamics (Akhmanova and Steinmetz, 2015). This is the first direct evidence of a link between the +TIP network and tubulin polyglutamylation.

Most cellular and organismal phenotypes of microtubule PTM deficiencies are associated with stable microtubule structures such as cilia, flagella and axons. In particular, it is well established that a correct pattern of axonemal PTMs is essential for flagellar and axonemal architecture and cell motility (Alper et al., 2014; Gadadhar et al., 2017; Hong et al., 2018; Kubo et al., 2014, 2010). Mice lacking the deglutamylase CCP5 (also known as AGBL5) have defects in spermatogenesis and are infertile (Giordano et al., 2019; Lee et al., 2013). Biophysically, dysfunctional polyglutamylation leads to the loss of asymmetric airway ciliary beating patterns or even stalled beating of mice sperm flagella (Ikegami et al., 2010; Konno et al., 2016). It has been shown that one possible consequence of impaired axonemal glutamylation is a defective interaction between tubulin and proteins of the inner-arm dynein regulatory complex (Kubo and Oda, 2017). Our data show that an imbalance in axonemal glutamylation PTMs in trypanosomes correlates with a severe motility defect. At present, we cannot conclude that the defect in flagellar polyglutamylation is causative for the motility defect or whether subtle changes in cell body dynamics are also involved. The precise mechanisms of how polyglutamylation affects flagellar function in trypanosomes remains to be determined. The trypanosome axonemal structure and proteome is evolutionarily highly conserved and has, for example, been established as a useful model system to study the molecular basis of certain ciliopathies (Coutton et al., 2018; Dawe et al., 2005, 2007). Here we show that trypanosomes are well suited as a system to analyse the functions of tubulin PTMs in relation to flagellar biology, an area pertinent to human diseases (Nsota Mbango et al., 2019).

In summary, our data show that microtubule post-translational polyglutamylation is a key parameter in the regulation of cytoskeletal architecture, cell shape and motility in trypanosomes. This process affects other events essential for cellular integrity, such as microtubule assembly dynamics and recruitment of other cytoskeletal regulatory proteins.

MATERIALS AND METHODS

Cell culture

Procyclic *T. brucei* 427 29-13 (TetR, T7RNAP) (Wirtz and Clayton, 1995), was maintained in SDM-79 medium (Life Technologies, UK) supplemented with 10% fetal bovine serum, 15 µg/ml G418 and 50 µg/ml hygromycin at 27°C. Cell growth was measured using a CASY cell counter (Roche Innovatis AG, Germany).

Generation of TbTTLL6A- and TbTTLL12B-RNAi cell lines

The RNAi constructs, pFC4-TbTTLL6A and pFC4-TbTTLL12B were created using the stem loop vector pFC4, which allows the doxycycline-inducible production of hairpin dsRNA with the use of a single doxycycline-inducible procyclin promotor (Bochud-Allemann and Schneider, 2002). DNA sequences for TbTTLL6A (*Tb927.3.5380*) and TbTTLL12B (*Tb927.11.2420*) were retrieved from TriTrypDB (https://tritrypdb.org/tritrypdb/). For pFC4-TbTTLL6A, a 266 bp DNA fragment was amplified using the sense primer TbTTLL6A_for and the anti-sense primer TbTTLL6A_rev. For pFC4-TbTTLL12B, a 180 bp fragment was amplified using the sense primer TbTTLL12B-RNAi_for and the anti-sense primer TbTTLL12B_rev. To avoid off-target effects, suitable RNAi targets were selected using the RNAit software (Redmond et al., 2003). The PCR products were cloned into the RNAi vector using the restriction sites HindIII, XbaI, XhoI and BamHI. The final constructs were linearised using NotI and transfected into procyclic cells by electroporation in an Amaxa Nucleofector II (Lonza, Germany) (Burkard et al., 2007). Transformants were selected using 10 µg/ml blasticidin. RNAi was induced using 1 µg/ml doxycycline. The primer sequences were as follows: TbTTLL6A_for, 5′-ATAGGATCCAAGCTTCTCTTCTCGGCGCCAAGTGT-3′; TbTTLL6-A_rev, 5′-ATACTCGAGTCTAGAAACGCCTTAACGTTGGCGAC-3′; TbTTLL12B_for, 5′-ATAGGATCCAAGCTTTCGGTGGAAGTTTGAA-GCTA-3′; TbTTLL12B_rev, 5′-ATACTCGAGTCTAGAAATGCTTCA-AAGTCTTTCAT-3′.

Sample preparation and western blotting

Cytoskeletons were prepared by whole cell extraction at 4°C for 30 min in extraction buffer [1 mM PIPES pH 6.9, 5 mM EDTA, 1 mM DTT and 1% (v/v) NP40]. Pelleted cytoskeletons were dissolved in hot SDS sample buffer [125 mM Tris-HCL pH 6.8, 5% (v/v) glycerol, 4% (v/v) SDS, 5% β-mercaptoethanol, some crystals of Bromophenol Blue] and boiled for 10 min. The equivalent of 2.5×10^4 cells per lane were loaded onto a 10% SDS gel. Proteins were transferred to nitrocellulose membrane and probed with primary and HRP-conjugated secondary antibodies. Blots were developed using chemiluminescence with Lumigen substrate (Lumigen, USA) on an ImageQuant LAS-4000 detection system (GE Healthcare, USA). Flagella were isolated using the sodium chloride extraction method, as described previously (Robinson et al., 1991).

Antibodies

Primary antibodies: mouse monoclonal anti-polyglutamylation modification (GT335; Biomol GmbH, Germany), final dilution 1:10,000 (for western blotting, WB), 1:6000 (for immunofluorescence, IF); rabbit polyclonal anti-polyglutamate chain (PolyE; Biomol GmbH), final dilution 1:10,000 (WB), 1:6000 (IF); anti-α tubulin (TAT) 2.81 mg/ml, final dilution 1:6000 (WB), 1:2000 (IF); anti-PFRA (L8C4) hybridoma supernatant, final dilution 1:50 (WB); anti-CAP5.5 hybridoma supernatant, final dilution 1:50

(WB) (TAT, L8C4 and CAP5.5 antibodies were gifts from Keith Gull, University of Oxford, UK); and anti-tyrosinated α-tubulin (YL1/2), hybridoma supernatant 1:50 (IF). A mouse monoclonal anti *T. brucei* EB1 antibody was prepared as follows: full-length *T. brucei* EB1 homologue (Tb927.9.2760) was cloned into pET28-His_6-SUMO1 (a gift from Olaf Stemmann, University of Bayreuth, Germany) and expressed in *E.coli* BL21(DE3)pLysS, purified under denaturing conditions on Ni-NTA resin (Qiagen, Germany) and used to immunise female BALB/c mice (Janvier Labs, France). After a routine immunisation scheme, spleen cells were isolated and fused to P3X63-Ag8.653 myeloma cells using polyethylene glycol 4000 and plated into 24-well plates containing Opti-MEM, 5% FCS, and hypoxanthine, aminopterin and thymidine (ThermoFisher–Gibco, Germany) and mouse peritoneal macrophage feeder cells. Supernatants were screened by immunofluorescence on *T. brucei* cytoskeletons for posterior cell tip staining. Positive wells were further subcloned by limiting dilution. The antibody isotype was determined using the Isostrip mouse mAb typing kit (Roche, Germany) and is of IgM isotype. Hybridoma supernatant was used at 1:50 dilution for immunofluorescence, and at 1:5 for western blotting.

Secondary antibodies: Anti-mouse IgG–HRP conjugate (Sigma Aldrich; Cat. No. A9044), final dilution 1:80,000; anti rabbit IgG–HRP conjugate (Invitrogen; Cat. No. 65-6120), final dilution 1:25,000; anti-mouse IgG–Atto 488 conjugate (Sigma Aldrich; Cat. No. 41698), final dilution 1:500; anti-rabbit IgG–Alexa Fluor 594 conjugate (Molecular Probes; Cat. No. A-21207), final dilution 1:1000; anti-rat IgG–Alexa Fluor 488 conjugate (Invitrogen), final dilution 1:1000 (IF).

Immunofluorescence microscopy

T. brucei cells were washed in PBS and settled onto poly-L-lysine-coated slides. For the preparation of cytoskeletons, cells were detergent extracted for 2 min with cold PEME (0.1 M PIPES pH 6.9, 2 mM EGTA, 1 mM $MgSO_4$ and 0.1 mM EDTA) containing 1% NP40. Cells were fixed in ice-cold methanol for at least 30 min. After rehydration in PBS, slides were incubated with the primary antibody for 1 h in a moist chamber. The slides were washed three times for 5 min in PBS and incubated with the secondary antibody for 1 h. Then, slides were washed twice in PBS; between washing steps the slides were incubated with DAPI (1 µg/ml in PBS) for 5 min. Cells were mounted in Vectashield Antifade Mounting Medium (Vector Labs). Imaging was done using a Zeiss Axio Imager M2 microscope equipped with a SPOT Pursuit CCD camera (Diagnostic Instruments) and recorded with VisiView Imaging software (Visitron, Germany).

Electron microscopy of whole-mount cytoskeletons

For whole-mount cytoskeletons, cells were washed in PBS and settled on pioloform-coated size 100 mesh copper grids (Plano GmbH, Wetzlar, Germany) in a moist chamber. For cytoskeleton preparations, cells were extracted with PEME containing 1% NP40 for 10 min at room temperature. Grids were washed with PEME three times. For fixation and negative staining, cells were incubated with 2% uranyl acetate for 1 min, washed with H_2O and stored on filter paper. Images were acquired using a JEM-1400 Plus electron microscope (JEOL, Germany) with a Ruby CCD camera (JEOL, Germany).

Quantification and statistical analyses

Quantification of western blots, fluorescence images and cellular phenotypes was performed using the image analysis software ImageJ v1.51h (https://imagej.nih.gov/ij/). For western blots the plug-in 'Analyze Gels' was used. Data were normalised to signal from the mouse monoclonal anti-α-tubulin antibody TAT. To quantify images and phenotypes the plug-in 'Analyze measure' was used. Statistical analyses were performed using the Past v3.24 software package (Hammer et al., 2001).

Motility assays

To analyse the movement of cells, 10 µl of a 3×10^6 cells/ml culture were transferred onto the non-gridded section of a Thoma chamber (depth 0.1 mm) and covered with a standard glass coverslip. As a reference point for non-motile *T. brucei*, live procyclic cells were settled and attached onto poly-L-lysine-coated coverslips.

Time-resolved bright-field illumination imaging of individual trypanosomes was performed at room temperature using a Leica DMI 6000 microscope (Leica Microsystems, Wetzlar Germany). Images were acquired with a monochrome digital CCD camera DFC360FX using a 20×/0.70 NA IMM air immersion objective, providing a large field of view (448.9 µm×335.2 µm). The setup was controlled using the Leica Application Suite X (LAS X, 3.6.0.20104).

Imaging was performed at a frequency of ten frames per second over a total period of 3 min, yielding 1800 frames, each with a camera exposure time of 5 ms. To achieve a representative sampling of the available motion patterns, at least three different regions were selected for each condition, in each of which at least five individuals were monitored. Samples were imaged for a maximum of 30 min after preparation to prevent ageing processes that perturb the motion pattern.

Image processing and single-particle tracking

For convenience, intensity values of all images were inverted before tracking the movement of kinetoplastids using FIJI (https://imagej.net/Fiji). For background correction, the mean of a region without *Trypanosoma* traces was determined in every image and then subtracted from the image. For improved tracking, the contrast of these background-corrected images was enhanced by allowing for 0.3% of all pixels to be saturated.

Trajectories were extracted from image stacks via the TrackMate plug-in for FIJI. Due to the transformations outlined in the previous paragraph, the contours of the parasite were approximately a blob with diameter of 8±1 µm. Therefore, tracking was performed using the Laplacian-of-Gaussian algorithm with a blob diameter of 24±2 pixels (~8 µm), a threshold set to 0.1±0.02, and median filter and sub-pixel localisation switched on. The centre-of-mass positions found with this approach were then linked with the linear assignment problem (LAP) tracker (Jaqaman et al., 2008). In the algorithm, a maximum linking distance and a maximum gap-closing distance of 2 µm was used, and the gap-closing maximum frame gap was set to 2.

The minimum length of trajectories was chosen to cover at least 5 s, i.e. $N\geq50$ positions, and no gaps were allowed in these tracks. To prevent artefacts from edge effects, all trajectories with a centre of mass closer than 3 µm to any edge were discarded. To rule out dead, stuck or overall immobile specimens, a minimum track displacement of 3 µm was used for all conditions except for lysine-coated dishes (in which trypanosomes were expected to be stuck). Tracks with N=100 positions and frame time Δt=100 ms, as well as all associated metadata, were exported as CSV and XML files, respectively. Subsequently, tracks were converted to ASCII files and analysed in Matlab using custom-written codes with respect to the measures given below. Here, only trajectories with a scaling exponent $\alpha\geq0.075$ in the mean squared displacement were retained for the complete analysis to exclude immobile tracks. As a result, for wild-type trypanosomes in unconstrained conditions, a total of 187 tracks were analysed; for wild-type trypanosomes on lysine-coated dishes 471 tracks were considered. For TTLL6A-RNAi (TTLL12B-RNAi) trypanosomes we analysed 352 (15) tracks from three experiments in the non-induced case, whereas 28 (61) tracks of RNAi-induced trypanosomes were considered.

For each of these two-dimensional trajectories: $\boldsymbol{r}(t) = \boldsymbol{r}(i\Delta t) = \boldsymbol{r}_i$ (with i=1,…,N denoting successive frames), we determined the time-averaged mean squared displacement (TA-MSD) for all possible lag times: $\tau = k\Delta t$, defined using Eqn 1:

$$\langle r^2(\tau)\rangle_t = \frac{1}{N-k}\sum_{i=1}^{N-k}\{\boldsymbol{r_{i+k}} - \boldsymbol{r_i}\}^2. \quad (1)$$

Individual TA-MSDs were fitted using a power law: $\langle r^2(\tau)\rangle_t = K_\alpha\tau^\alpha$, in the range $\Delta t\leq\tau\leq10\Delta t$ to extract the generalised diffusion coefficient, K_α, and the scaling exponent α. Normal Brownian diffusion is indicated by $\alpha=1$, whereas sub- and super-diffusive motion is highlighted by $\alpha<1$ and $\alpha>1$, respectively. Histograms of the obtained set of scaling exponents approximate, after appropriate normalisation, the probability density function (PDF) $P(\alpha)$ for each condition. In all cases, a two-sample Kolmogorov–Smirnov test was used to probe the significance level between different conditions.

As a second measure we determined for each trajectory the taken step lengths $\delta r_i = |r_{i+5} - r_i|$ between frames separated by a time increment $\delta t = 5\Delta t$. Due to the discreteness of the trajectory, the obtained set of step lengths also yielded a set of (positive) instantaneous velocities $v_i = \delta r_i/\delta t$. Grouping together all instantaneous velocities from all trajectories from the same conditions yielded the PDF $P(v)$, whose mean quantifies the ensemble-averaged travel velocity $\langle v \rangle$ of trypanosomes at the respective condition.

Because both of the two aforementioned quantities only test for the overall mobility but not to what extent a directional movement is observed, we also employed the straightness (S) of individual tracks as an additional criterion, defined using Eqn 2:

$$S_i = \frac{|\boldsymbol{r}_{i+n} - \boldsymbol{r}_i|}{\sum_{j=i+1}^{i+n} |\boldsymbol{r}_j - \boldsymbol{r}_{j-1}|}. \quad (2)$$

Using a sliding window approach (window size n=15) and assuming stationarity we combined all values of S (i.e. each window of each trajectory at the same condition) into a single PDF, $P(S)$. It is worth noting that S is a self-normalising quantity and therefore does not need any additional normalisation when comparing different conditions.

Acknowledgements
We thank Markus Spindler for preparing recombinant EB1 protein, Nina Salein for making the RNAi constructs, Rita Grotjahn for assistance with electron microscopy and Benedikt Westermann for comments on the manuscript.

Competing interests
The authors declare no competing or financial interests.

Author contributions
Conceptualization: K.E.; Methodology: J.J., K.E.; Software: A.S.; Validation: J.J., A.S., K.E.; Formal analysis: J.J., A.S.; Investigation: J.J., A.S., K.S., G.L.-K.; Writing - original draft: M.W., K.E.; Visualization: J.J., A.S.; Supervision: M.W., K.E.; Project administration: K.E.; Funding acquisition: M.W., K.E.

Funding
M.W., K.S., and A.S. gratefully acknowledge financial support by the Volkswagen Foundation (Az. 92738) and the Elitenetzwerk Bayern (Study Program Biological Physics).

Supplementary information
Supplementary information available online at
https://jcs.biologists.org/lookup/doi/10.1242/jcs.248047.supplemental

Peer review history
The peer review history is available online at
https://jcs.biologists.org/lookup/doi/10.1242/jcs.248047.reviewer-comments.pdf

References
Akhmanova, A. and Steinmetz, M. O. (2015). Control of microtubule organization and dynamics: two ends in the limelight. *Nat. Rev. Mol. Cell Biol.* **16**, 711-726. doi:10.1038/nrm4084

Alizadehrad, D., Krüger, T., Engstler, M. and Stark, H. (2015). Simulating the complex cell design of *Trypanosoma brucei* and its motility. *PLoS Comput. Biol.* **11**, e1003967. doi:10.1371/journal.pcbi.1003967

Alper, J. D., Decker, F., Agana, B. and Howard, J. (2014). The motility of axonemal dynein is regulated by the tubulin code. *Biophys. J.* **107**, 2872-2880. doi:10.1016/j.bpj.2014.10.061

Alsford, S., Turner, D. J., Obado, S. O., Sanchez-Flores, A., Glover, L., Berriman, M., Hertz-Fowler, C. and Horn, D. (2011). High-throughput phenotyping using parallel sequencing of RNA interference targets in the African trypanosome. *Genome Res.* **21**, 915-924. doi:10.1101/gr.115089.110

Badin-Larcon, A. C., Boscheron, C., Soleilhac, J. M., Piel, M., Mann, C., Denarier, E., Fourest-Lieuvin, A., Lafanechere, L., Bornens, M. and Job, D. (2004). Suppression of nuclear oscillations in *Saccharomyces cerevisiae* expressing Glu tubulin. *Proc. Natl. Acad. Sci. USA* **101**, 5577-5582. doi:10.1073/pnas.0307917101

Baines, A. and Gull, K. (2008). WCB is a C2 domain protein defining the plasma membrane - sub-pellicular microtubule corset of kinetoplastid parasites. *Protist* **159**, 115-125. doi:10.1016/j.protis.2007.09.001

Barra, H. S., Rodriguez, J. A., Arce, C. A. and Caputto, R. (1973). A soluble preparation from rat brain that incorporates into its own proteins [^{14}C]arginine by a ribonuclease-sensitive system and [^{14}C]tyrosine by a ribonuclease-insensitive system. *J. Neurochem.* **20**, 97-108. doi:10.1111/j.1471-4159.1973.tb12108.x

Basmaciyan, L., Robinson, D. R., Azas, N. and Casanova, M. (2019). (De)glutamylation and cell death in *Leishmania* parasites. *PLoS Negl. Trop. Dis.* **13**, e0007264. doi:10.1371/journal.pntd.0007264

Bieling, P., Kandels-Lewis, S., Telley, I. A., van Dijk, J., Janke, C. and Surrey, T. (2008). CLIP-170 tracks growing microtubule ends by dynamically recognizing composite EB1/tubulin-binding sites. *J. Cell Biol.* **183**, 1223-1233. doi:10.1083/jcb.200809190

Bigman, L. S. and Levy, Y. (2020). Tubulin tails and their modifications regulate protein diffusion on microtubules. *Proc. Natl. Acad. Sci. USA* **117**, 8876-8883. doi:10.1073/pnas.1914772117

Bochud-Allemann, N. and Schneider, A. (2002). Mitochondrial substrate level phosphorylation is essential for growth of procyclic *Trypanosoma brucei*. *J. Biol. Chem.* **277**, 32849-32854. doi:10.1074/jbc.M205776200

Bodakuntla, S., Jijumon, A. S., Villablanca, C., Gonzalez-Billault, C. and Janke, C. (2019). Microtubule-associated proteins: structuring the cytoskeleton. *Trends Cell Biol.* **29**, 804-819. doi:10.1016/j.tcb.2019.07.004

Broadhead, R., Dawe, H. R., Farr, H., Griffiths, S., Hart, S. R., Portman, N., Shaw, M. K., Ginger, M. L., Gaskell, S. J., McKean, P. G. et al. (2006). Flagellar motility is required for the viability of the bloodstream trypanosome. *Nature* **440**, 224-227. doi:10.1038/nature04541

Burkard, G., Fragoso, C. M. and Roditi, I. (2007). Highly efficient stable transformation of bloodstream forms of *Trypanosoma brucei*. *Mol. Biochem. Parasitol.* **153**, 220-223. doi:10.1016/j.molbiopara.2007.02.008

Casanova, M., de Monbrison, F., Van Dijk, J., Janke, C., Pagès, M. and Bastien, P. (2015). Characterisation of polyglutamylases in trypanosomatids. *Int. J. Parasitol.* **45**, 121-132. doi:10.1016/j.ijpara.2014.09.005

Coutton, C., Vargas, A. S., Amiri-Yekta, A., Kherraf, Z.-E., Ben Mustapha, S. F., Le Tanno, P., Wambergue-Legrand, C., Karaouzène, T., Martinez, G., Crouzy, S. et al. (2018). Mutations in CFAP43 and CFAP44 cause male infertility and flagellum defects in *Trypanosoma* and human. *Nat. Commun.* **9**, 686. doi:10.1038/s41467-017-02792-7

Dawe, H. R., Farr, H., Portman, N., Shaw, M. K. and Gull, K. (2005). The Parkin co-regulated gene product, PACRG, is an evolutionarily conserved axonemal protein that functions in outer-doublet microtubule morphogenesis. *J. Cell Sci.* **118**, 5421-5430. doi:10.1242/jcs.02659

Dawe, H. R., Shaw, M. K., Farr, H. and Gull, K. (2007). The hydrocephalus inducing gene product, Hydin, positions axonemal central pair microtubules. *BMC Biol.* **5**, 33. doi:10.1186/1741-7007-5-33

Dawson, S. C. and Paredez, A. R. (2013). Alternative cytoskeletal landscapes: cytoskeletal novelty and evolution in basal excavate protists. *Curr. Opin. Cell Biol.* **25**, 134-141. doi:10.1016/j.ceb.2012.11.005

Ddeberg, O. and Bertrand, J. (1998). Tubulin tyrosine ligase: a shared fold with the glutathione synthetase ADP-forming family. *Trends Biochem. Sci.* **23**, 57-58. doi:10.1016/S0968-0004(97)01149-3

Edde, B., Rossier, J., Le Caer, J. P., Desbruyeres, E., Gros, F. and Denoulet, P. (1990). Posttranslational glutamylation of alpha-tubulin. *Science* **247**, 83-85. doi:10.1126/science.1967194

Eipper, B. A. (1972). Rat brain microtubule protein: purification and determination of covalently bound phosphate and carbohydrate. *Proc. Natl. Acad. Sci. USA* **69**, 2283-2287. doi:10.1073/pnas.69.8.2283

Elmendorf, H. G., Dawson, S. C. and McCaffery, J. M. (2003). The cytoskeleton of *Giardia lamblia*. *Int. J. Parasitol.* **33**, 3-28. doi:10.1016/S0020-7519(02)00228-X

Engstler, M., Pfohl, T., Herminghaus, S., Boshart, M., Wiegertjes, G., Heddergott, N. and Overath, P. (2007). Hydrodynamic flow-mediated protein sorting on the cell surface of trypanosomes. *Cell* **131**, 505-515. doi:10.1016/j.cell.2007.08.046

Erck, C., Peris, L., Andrieux, A., Meissirel, C., Gruber, A. D., Vernet, M., Schweitzer, A., Saoudi, Y., Pointu, H., Bosc, C. et al. (2005). A vital role of tubulin-tyrosine-ligase for neuronal organization. *Proc. Natl. Acad. Sci. USA* **102**, 7853-7858. doi:10.1073/pnas.0409626102

Ersfeld, K., Wehland, J., Plessmann, U., Dodemont, H., Gerke, V. and Weber, K. (1993). Characterization of the tubulin-tyrosine ligase. *J. Cell Biol.* **120**, 725-732. doi:10.1083/jcb.120.3.725

Ersfeld, K., Asbeck, K. and Gull, K. (1998). Direct visualisation of individual gene organisation in *Trypanosoma brucei* by high-resolution *in situ* hybridisation. *Chromosoma* **107**, 237-240. doi:10.1007/s004120050302

Gadadhar, S., Dadi, H., Bodakuntla, S., Schnitzler, A., Bièche, I., Rusconi, F. and Janke, C. (2017). Tubulin glycylation controls primary cilia length. *J. Cell Biol.* **216**, 2701-2713. doi:10.1083/jcb.201612050

Giordano, T., Gadadhar, S., Bodakuntla, S., Straub, J., Leboucher, S., Martinez, G., Chemlali, W., Bosc, C., Andrieux, A., Bieche, I. et al. (2019). Loss of the deglutamylase CCP5 perturbs multiple steps of spermatogenesis and leads to male infertility. *J. Cell Sci.* **132**, jcs226951. doi:10.1242/jcs.226951

Gull, K. (1999). The cytoskeleton of trypanosomatid parasites. *Annu. Rev. Microbiol.* **53**, 629-655. doi:10.1146/annurev.micro.53.1.629

Hammarton, T. C., Engstler, M. and Mottram, J. C. (2004). The *Trypanosoma brucei* cyclin, CYC2, is required for cell cycle progression through G_1 phase and

for maintenance of procyclic form cell morphology. *J. Biol. Chem.* **279**, 24757-24764. doi:10.1074/jbc.M401276200

Hammer, Ø., Harper, D. A. T. and Ryan, P. D. (2001). PAST: paleontological statistics software package for education and data analysis. *Palaeontol. Electron.* **4**, 1-9.

Hemphill, A., Lawson, D. and Seebeck, T. (1991). The cytoskeletal architecture of *Trypanosoma brucei*. *J. Parasitol.* **77**, 603-612. doi:10.2307/3283167

Hendriks, E. F., Robinson, D. R., Hinkins, M. and Matthews, K. R. (2001). A novel CCCH protein which modulates differentiation of *Trypanosoma brucei* to its procyclic form. *EMBO J.* **20**, 6700-6711. doi:10.1093/emboj/20.23.6700

Hertz-Fowler, C., Ersfeld, K. and Gull, K. (2001). CAP5.5, a life-cycle-regulated, cytoskeleton-associated protein is a member of a novel family of calpain-related proteins in *Trypanosoma brucei*. *Mol. Biochem. Parasitol.* **116**, 25-34. doi:10.1016/S0166-6851(01)00296-1

Hong, S.-R., Wang, C.-L., Huang, Y.-S., Chang, Y.-C., Chang, Y.-C., Pusapati, G. V., Lin, C.-Y., Hsu, N., Cheng, H. C., Chiang, Y.-C. et al. (2018). Spatiotemporal manipulation of ciliary glutamylation reveals its roles in intraciliary trafficking and Hedgehog signaling. *Nat. Commun.* **9**, 1732. doi:10.1038/s41467-018-03952-z

Ikegami, K., Sato, S., Nakamura, K., Ostrowski, L. E. and Setou, M. (2010). Tubulin polyglutamylation is essential for airway ciliary function through the regulation of beating asymmetry. *Proc. Natl. Acad. Sci. USA* **107**, 10490-10495. doi:10.1073/pnas.1002128107

Janke, C. (2014). The tubulin code: molecular components, readout mechanisms, and functions. *J. Cell Biol.* **206**, 461-472. doi:10.1083/jcb.201406055

Janke, C., Rogowski, K., Wloga, D., Regnard, C., Kajava, A. V., Strub, J.-M., Temurak, N., Van Dijk, J., Boucher, D., van Dorsselaer, A. et al. (2005). Tubulin polyglutamylase enzymes are members of the TTL domain protein family. *Science* **308**, 1758-1762. doi:10.1126/science.1113010

Jaqaman, K., Loerke, D., Mettlen, M., Kuwata, H., Grinstein, S., Schmid, S. L. and Danuser, G. (2008). Robust single-particle tracking in live-cell time-lapse sequences. *Nat. Methods* **5**, 695-702. doi:10.1038/nmeth.1237

Kilmartin, J. V., Wright, B. and Milstein, C. (1982). Rat monoclonal antitubulin antibodies derived by using a new nonsecreting rat cell line. *J. Cell Biol.* **93**, 576-582. doi:10.1083/jcb.93.3.576

Konno, A., Ikegami, K., Konishi, Y., Yang, H.-J., Abe, M., Yamazaki, M., Sakimura, K., Yao, I., Shiba, K., Inaba, K. et al. (2016). *Ttll9*$^{-/-}$ mice sperm flagella show shortening of doublet 7, reduction of doublet 5 polyglutamylation and a stall in beating. *J. Cell Sci.* **129**, 2757-2766. doi:10.1242/jcs.185983

Kubo, T. and Oda, T. (2017). Electrostatic interaction between polyglutamylated tubulin and the nexin-dynein regulatory complex regulates flagellar motility. *Mol. Biol. Cell* **28**, 2260-2266. doi:10.1091/mbc.e17-05-0285

Kubo, T., Yanagisawa, H.-A., Yagi, T., Hirono, M. and Kamiya, R. (2010). Tubulin polyglutamylation regulates axonemal motility by modulating activities of inner-arm dyneins. *Curr. Biol.* **20**, 441-445. doi:10.1016/j.cub.2009.12.058

Kubo, T., Yanagisawa, H.-A., Liu, Z., Shibuya, R., Hirono, M. and Kamiya, R. (2014). A conserved flagella-associated protein in *Chlamydomonas*, FAP234, is essential for axonemal localization of tubulin polyglutamylase TTLL9. *Mol. Biol. Cell* **25**, 107-117. doi:10.1091/mbc.e13-07-0424

Langousis, G. and Hill, K. L. (2014). Motility and more: the flagellum of *Trypanosoma brucei*. *Nat. Rev. Microbiol.* **12**, 505-518. doi:10.1038/nrmicro3274

Lee, G.-S., He, Y., Dougherty, E. J., Jimenez-Movilla, M., Avella, M., Grullon, S., Sharlin, D. S., Guo, C., Blackford, J. A., Jr, Awasthi, S. et al. (2013). Disruption of Ttll5/stamp gene (tubulin tyrosine ligase-like protein 5/SRC-1 and TIF2-associated modulatory protein gene) in male mice causes sperm malformation and infertility. *J. Biol. Chem.* **288**, 15167-15180. doi:10.1074/jbc.M113.453936

Magiera, M. M., Bodakuntla, S., Žiak, J., Lacomme, S., Marques Sousa, P., Leboucher, S., Hausrat, T. J., Bosc, C., Andrieux, A., Kneussel, M. et al. (2018). Excessive tubulin polyglutamylation causes neurodegeneration and perturbs neuronal transport. *EMBO J.* **37**, e100440. doi:10.15252/embj.2018100440

Matthews, K. R., Sherwin, T. and Gull, K. (1995). Mitochondrial genome repositioning during the differentiation of the African trypanosome between life cycle forms is microtubule mediated. *J. Cell Sci.* **108**, 2231-2239.

Morrissette, N. S. and Sibley, L. D. (2002). Cytoskeleton of apicomplexan parasites. *Microbiol. Mol. Biol. Rev.* **66**, 21-38. doi:10.1128/MMBR.66.1.21-38.2002

Nehlig, A., Molina, A., Rodrigues-Ferreira, S., Honoré, S. and Nahmias, C. (2017). Regulation of end-binding protein EB1 in the control of microtubule dynamics. *Cell. Mol. Life Sci.* **74**, 2381-2393. doi:10.1007/s00018-017-2476-2

Nsota Mbango, J. F., Coutton, C., Arnoult, C., Ray, P. F. and Touré, A. (2019). Genetic causes of male infertility: snapshot on morphological abnormalities of the sperm flagellum. *Basic Clin. Androl.* **29**, 2. doi:10.1186/s12610-019-0083-9

Olego-Fernandez, S., Vaughan, S., Shaw, M. K., Gull, K. and Ginger, M. L. (2009). Cell morphogenesis of *Trypanosoma brucei* requires the paralogous, differentially expressed calpain-related proteins CAP5.5 and CAP5.5V. *Protist* **160**, 576-590. doi:10.1016/j.protis.2009.05.003

Pasternack, D. A., Sharma, A. I., Olson, C. L., Epting, C. L. and Engman, D. M. (2015). Sphingosine kinase regulates microtubule dynamics and organelle positioning necessary for proper G1/S cell cycle transition in *Trypanosoma brucei*. *mBio* **6**, e01291-15. doi:10.1128/mBio.01291-15

Peris, L., Thery, M., Fauré, J., Saoudi, Y., Lafanechère, L., Chilton, J. K., Gordon-Weeks, P., Galjart, N., Bornens, M., Wordeman, L. et al. (2006). Tubulin tyrosination is a major factor affecting the recruitment of CAP-Gly proteins at microtubule plus ends. *J. Cell Biol.* **174**, 839-849. doi:10.1083/jcb.200512058

Raybin, D. and Flavin, M. (1977). Modification of tubulin by tyrosylation in cells and extracts and its effect on assembly in vitro. *J. Cell Biol.* **73**, 492-504. doi:10.1083/jcb.73.2.492

Redeker, V., Levilliers, N., Schmitter, J. M., Le Caer, J. P., Rossier, J., Adoutte, A. and Bré, M. H. (1994). Polyglycylation of tubulin: a posttranslational modification in axonemal microtubules. *Science* **266**, 1688-1691. doi:10.1126/science.7992051

Redmond, S., Vadivelu, J. and Field, M. C. (2003). RNAit: an automated web-based tool for the selection of RNAi targets in *Trypanosoma brucei*. *Mol. Biochem. Parasitol.* **128**, 115-118. doi:10.1016/S0166-6851(03)00045-8

Robinson, D. R. and Gull, K. (1991). Basal body movements as a mechanism for mitochondrial genome segregation in the trypanosome cell cycle. *Nature* **352**, 731-733. doi:10.1038/352731a0

Robinson, D., Beattie, P., Sherwin, T. and Gull, K. (1991). Microtubules, tubulin, and microtubule-associated proteins of trypanosomes. *Methods Enzymol.* **196**, 285-299. doi:10.1016/0076-6879(91)96027-O

Robinson, D. R., Sherwin, T., Ploubidou, A., Byard, E. H. and Gull, K. (1995). Microtubule polarity and dynamics in the control of organelle positioning, segregation, and cytokinesis in the trypanosome cell cycle. *J. Cell Biol.* **128**, 1163-1172. doi:10.1083/jcb.128.6.1163

Rotureau, B., Ooi, C.-P., Huet, D., Perrot, S. and Bastin, P. (2014). Forward motility is essential for trypanosome infection in the tsetse fly. *Cell. Microbiol.* **16**, 425-433. doi:10.1111/cmi.12230

Sasse, R. and Gull, K. (1988). Tubulin post-translational modifications and the construction of microtubular organelles in *Trypanosoma brucei*. *J. Cell Sci.* **90**, 577-589.

Schneider, A., Plessmann, U. and Weber, K. (1997). Subpellicular and flagellar microtubules of *Trypanosoma brucei* are extensively glutamylated. *J. Cell Sci.* **110**, 431-437.

Shang, Y., Li, B. and Gorovsky, M. A. (2002). *Tetrahymena thermophila* contains a conventional gamma-tubulin that is differentially required for the maintenance of different microtubule-organizing centers. *J. Cell Biol.* **158**, 1195-1206. doi:10.1083/jcb.200205101

Sheriff, O., Lim, L.-F. and He, C. Y. (2014). Tracking the biogenesis and inheritance of subpellicular microtubule in *Trypanosoma brucei* with inducible YFP-alpha-tubulin. *Biomed. Res. Int.* **2014**, 893272. doi:10.1155/2014/893272

Sherwin, T. and Gull, K. (1989). Visualization of detyrosination along single microtubules reveals novel mechanisms of assembly during cytoskeletal duplication in trypanosomes. *Cell* **57**, 211-221. doi:10.1016/0092-8674(89)90959-8

Sherwin, T., Schneider, A., Sasse, R., Seebeck, T. and Gull, K. (1987). Distinct localization and cell cycle dependence of COOH terminally tyrosinolated alpha-tubulin in the microtubules of *Trypanosoma brucei brucei*. *J. Cell Biol.* **104**, 439-446. doi:10.1083/jcb.104.3.439

Sinclair, A. N. and de Graffenried, C. L. (2019). More than microtubules: the structure and function of the subpellicular array in trypanosomatids. *Trends Parasitol.* **35**, 760-777. doi:10.1016/j.pt.2019.07.008

Thomashow, L. S., Milhausen, M., Rutter, W. J. and Agabian, N. (1983). Tubulin genes are tandemly linked and clustered in the genome of *Trypanosoma brucei*. *Cell* **32**, 35-43. doi:10.1016/0092-8674(83)90494-4

Uppaluri, S., Heddergott, N., Stellamanns, E., Herminghaus, S., Zöttl, A., Stark, H., Engstler, M. and Pfohl, T. (2012). Flow loading induces oscillatory trajectories in a bloodstream parasite. *Biophys. J.* **103**, 1162-1169. doi:10.1016/j.bpj.2012.08.020

van der Laan, S., Leveque, M. F., Marcellin, G., Vezenkov, L., Lannay, Y., Dubra, G., Bompard, G., Ovejero, S., Urbach, S., Burgess, A. et al. (2019). Evolutionary divergence of enzymatic mechanisms for tubulin detyrosination. *Cell Rep.* **29**, 4159-4171.e6.

van Dijk, J., Rogowski, K., Miro, J., Lacroix, B., Edde, B. and Janke, C. (2007). A targeted multienzyme mechanism for selective microtubule polyglutamylation. *Mol. Cell* **26**, 437-448. doi:10.1016/j.molcel.2007.04.012

van Dijk, J., Miro, J., Strub, J.-M., Lacroix, B., van Dorsselaer, A., Edde, B. and Janke, C. (2008). Polyglutamylation is a post-translational modification with a broad range of substrates. *J. Biol. Chem.* **283**, 3915-3922. doi:10.1074/jbc.M705813200

Vedrenne, C., Giroud, C., Robinson, D. R., Besteiro, S., Bosc, C., Bringaud, F. and Baltz, T. (2002). Two related subpellicular cytoskeleton-associated proteins in *Trypanosoma brucei* stabilize microtubules. *Mol. Biol. Cell* **13**, 1058-1070. doi:10.1091/mbc.01-06-0298

Westermann, S. and Weber, K. (2003). Post-translational modifications regulate microtubule function. *Nat. Rev. Mol. Cell Biol.* **4**, 938-948. doi:10.1038/nrm1260

Wirtz, E. and Clayton, C. (1995). Inducible gene expression in trypanosomes mediated by a prokaryotic repressor. *Science* **268**, 1179-1183. doi:10.1126/science.7761835

Wloga, D., Webster, D. M., Rogowski, K., Bré, M.-H., Levilliers, N., Jerka-Dziadosz, M., Janke, C., Dougan, S. T. and Gaertig, J. (2009). TTLL3 Is a tubulin glycine ligase that regulates the assembly of cilia. *Dev. Cell* **16**, 867-876. doi:10.1016/j.devcel.2009.04.008

Wloga, D., Joachimiak, E. and Fabczak, H. (2017). Tubulin post-translational modifications and microtubule dynamics. *Int. J. Mol. Sci.* **18**, 2207. doi:10.3390/ijms18102207

Wolff, A., de Néchaud, B., Chillet, D., Mazarguil, H., Desbruyères, E., Audebert, S., Eddé, B., Gros, F. and Denoulet, P. (1992). Distribution of glutamylated alpha and beta-tubulin in mouse tissues using a specific monoclonal antibody, GT335. *Eur. J. Cell Biol.* **59**, 425-432.

Woods, A., Sherwin, T., Sasse, R., MacRae, T. H., Baines, A. J. and Gull, K. (1989). Definition of individual components within the cytoskeleton of *Trypanosoma brucei* by a library of monoclonal antibodies. *J. Cell Sci.* **93**, 491-500.

Yubuki, N., Čepička, I. and Leander, B. S. (2016). Evolution of the microtubular cytoskeleton (flagellar apparatus) in parasitic protists. *Mol. Biochem. Parasitol.* **209**, 26-34. doi:10.1016/j.molbiopara.2016.02.002

Zaburdaev, V., Uppaluri, S., Pfohl, T., Engstler, M., Friedrich, R. and Stark, H. (2011). Langevin dynamics deciphers the motility pattern of swimming parasites. *Phys. Rev. Lett.* **106**, 208103. doi:10.1103/PhysRevLett.106.208103

Table S1

Nomenclature of Tubulin-Tyrosine Ligase (TTL) and Tubulin-Tyrosine-Ligase-Like (TTLL) proteins in *Trypanosoma brucei*

(modified after Casanova et al.)[1]

TTLL code	Gene ID
TTL-A	Tb927.2.5250
TTLL1	Tb927.5.3860
TTLL4A	Tb927.9.9580
TTLL4B	Tb927.6.3570
TTLL4C	Tb927.1.1550
TTLL6A	Tb927.3.5380
TTLL6B	Tb927.11.6810
TTLL9	Tb927.10.13870
TTLL12B	Tb927.11.2420

TTLL proteins of this study are highlighted

[1] Casanova, M. *et al.* Characterisation of polyglutamylases in trypanosomatids. *Int J Parasitol* **45,** 121–132 (2015).

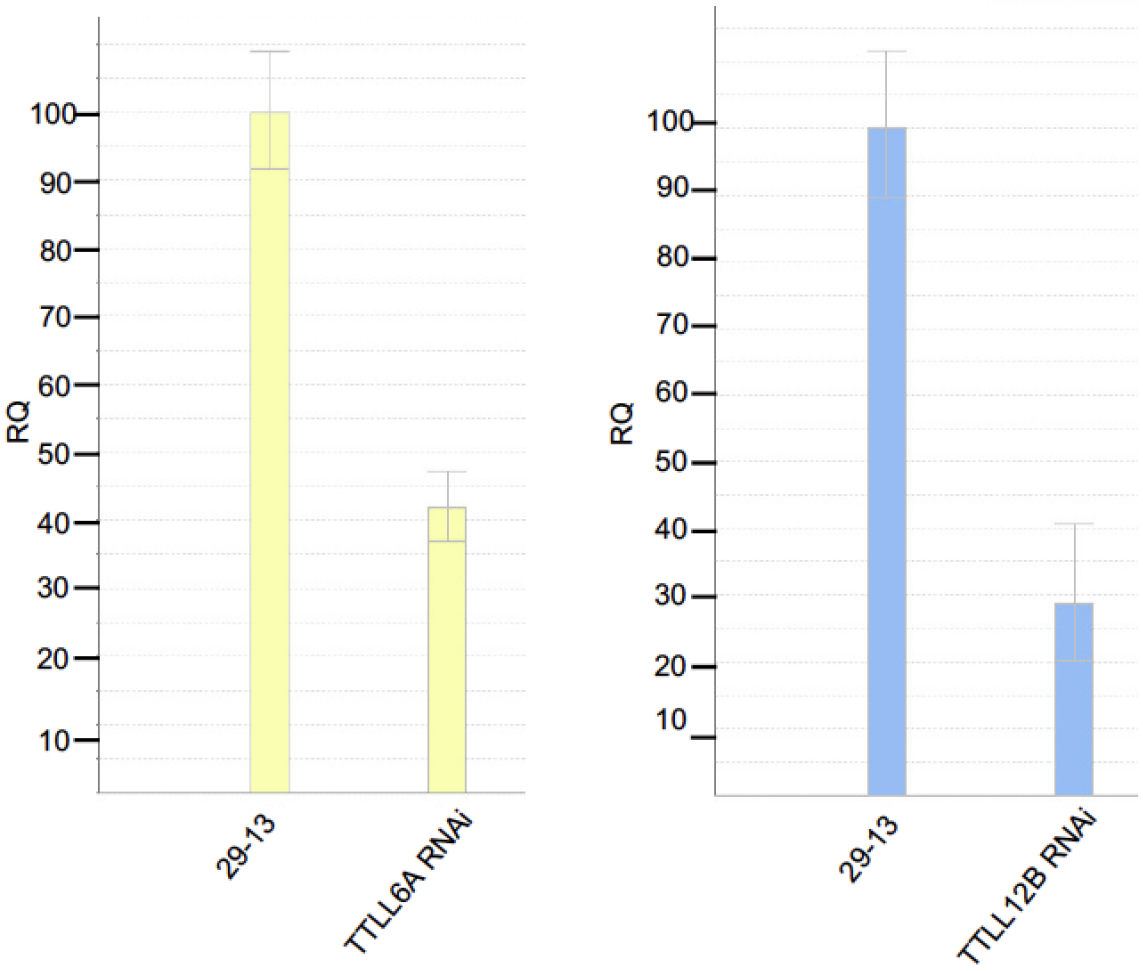

Fig. S1. RNAi efficiency of TTLL6A and TTLL12B knockdown. RNAi efficiency was measured using quantitative real-time PCR. Knockdown of TTLL6A (TTLL6A-RNAi) reduced mRNA level to 60 % compared to the parental cell line (29-13). Knockdown of TTLL12B (TTLL12B-RNAi) reduced mRNA level to 70 % compared to the parental cell line (29-13). RNAi cells were 24h induced. RQ = relative mRNA expression level (%).

Method: RNA was isolated using the Qiagen RNeasy Mini Kit and treated with the DNA-free kit (Invitrogen) to remove contaminating genomic DNA. RNA was reverse-transcribed to cDNA using the RevertAid First Strand cDNA synthesis kit (Thermo Fisher Scientific). qPCR was performed using the Maxima SYBR Green/ROX qPCR Master Mix (Thermo Fisher Scientific) on a Step One real time PCR system (Applied Biosystems). Samples were calculated with the $\Delta\Delta C_T$-method. The constitutively expressed transcript for the paraflagellar rod protein A (PFRA) was used as reference for normalisation. Primers for TbTTLL6A and TTLL12B were the same as for generating the RNAi fragments (see Main text, Material and Methods). For PFRA primer sequences were: PFRA_For 5' CGTTGGAGATGTTTGGACCT; PFRA_Rev 5' GCACGGTACTCCACCATCTT

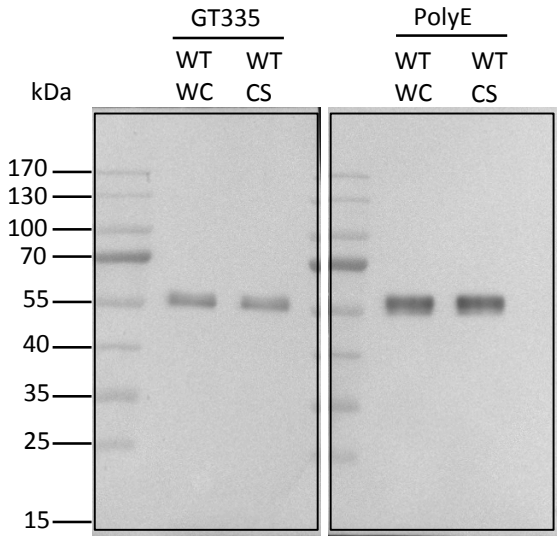

Fig. S2. Binding patterns of the antibodies GT335 and PolyE on western blots. Western blots of whole cell lysates (WC) and cytoskeletons lysates (CS) of wild type cells (29-13) probed with the antibodies GT335 (recognizes the branching point of glutamyl side chains) and PolyE (recognizes glutamyl side chains with at least four glutamate residues).

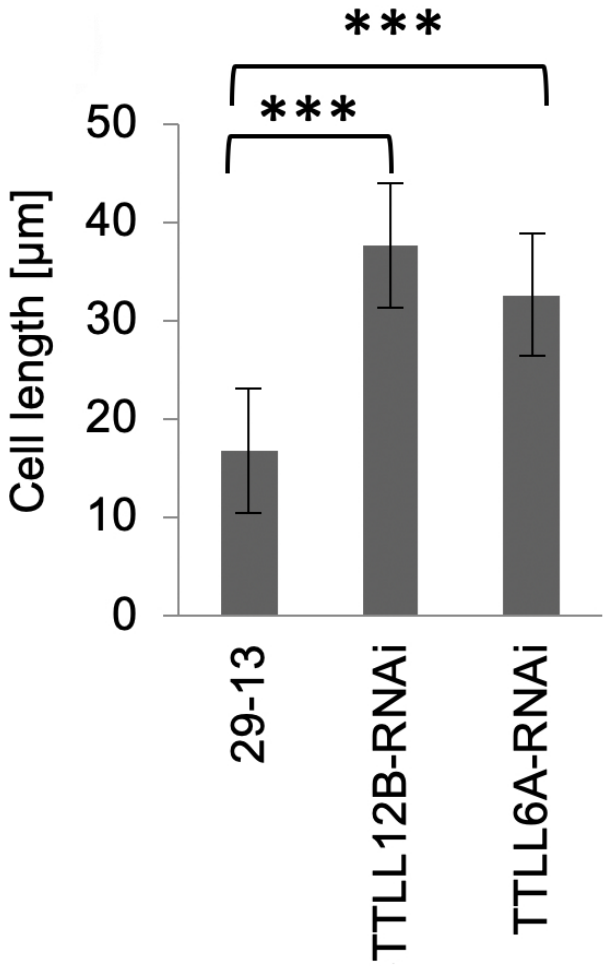

Fig. S3. Length analysis of TTLL6A or TTLL12B depleted cells. Cell length of wild type cells (29-13) and RNAi cells after two days induction were measured. Statistically significant differences compared with the wild type cells are indicated (Kolmogorov-Smirnov, *P < 0,05; ***P < 0,001). n=10. Error bars indicate the standard error.

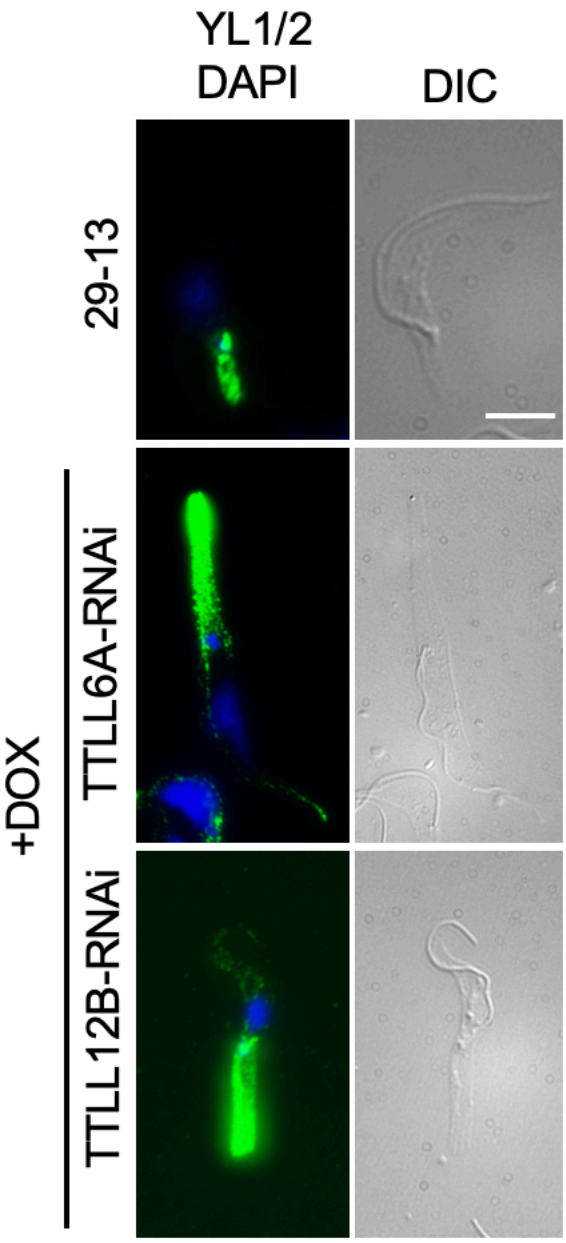

Fig. S4. Effect of TTLL6A and TTLL12B depletion on the distribution of tyrosinated microtubules and localisation of end-binding protein EB1. Immunofluorescence images of cytoskeletons of wild type cells (29-13) and RNAi cells (TTLL6A-RNAi, TTLL12B-RNAi) after two days induction. Tyrosinated α tubulin was stained with YL1/2 (green), nuclear and kinetoplast DNA

was stained with DAPI (blue). In contrast to Fig. 3, a 5-fold higher concentration of YL1/2 was used. This displays the typical posterior staining of wild-type T. *brucei* described in the literature (see Sherwin et al. 1987). However, the strong increase of staining intensity in TTLL-depleted cells is still clearly visible.

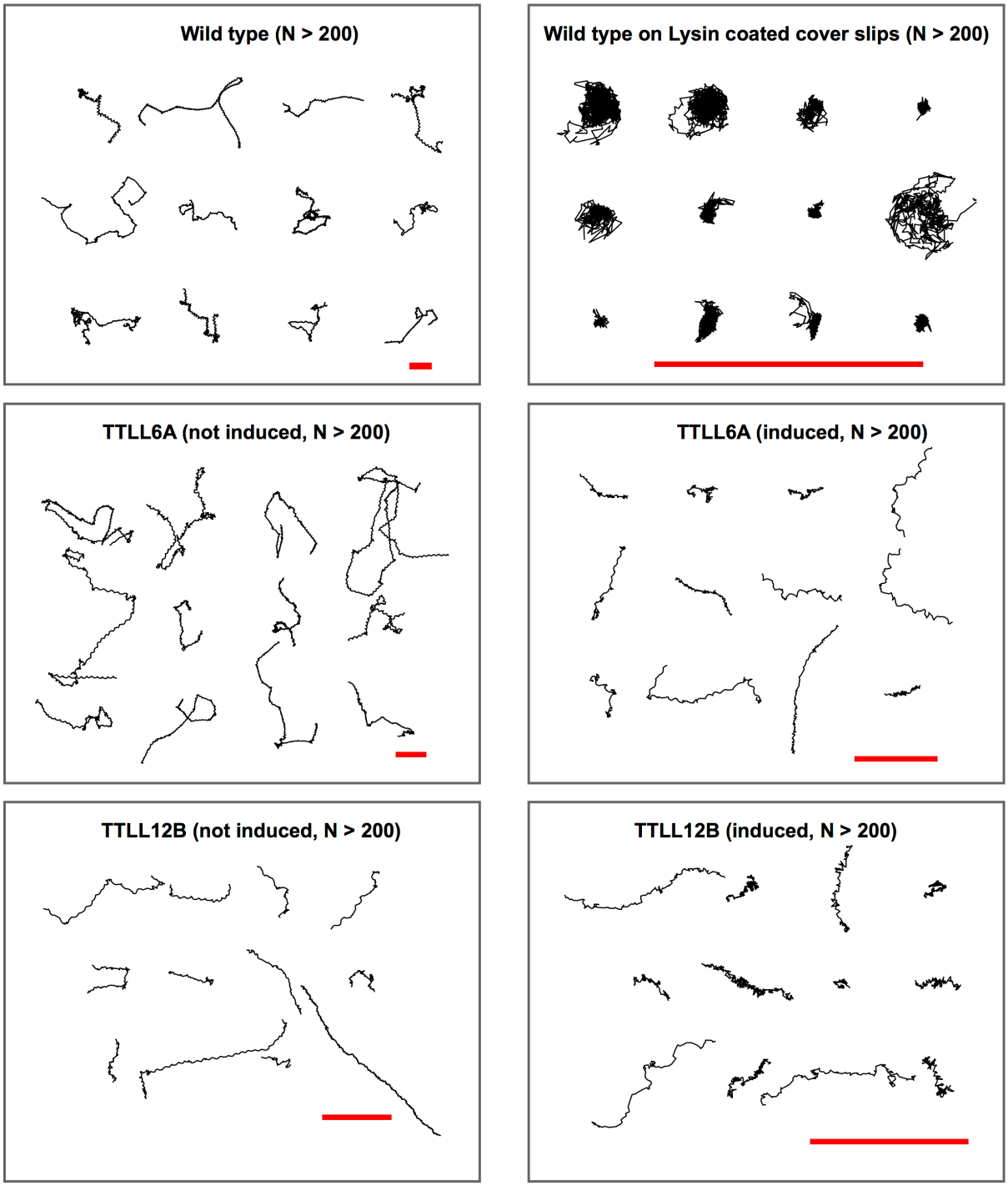

Fig. S5. Typical trajectories of trypanosomes with N=200 positions for the indicated conditions. Red scale bars in each frame represent 200µm, highlighting the varying diameters of trajectories for the various conditions.

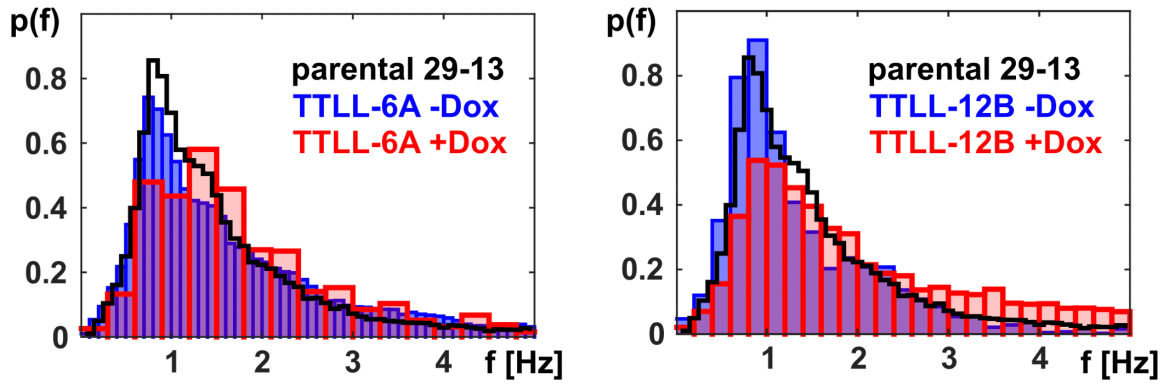

Fig. S6. The PDF of the helical frequency of trypanosome motion, p(f), as determined from individual trajectories.

Extraction of helical frequencies was performed as follows: Two-dimensional trajectories with at least N=200 positions were first divided into segments of length w=50. Each segment was then linearly interpolated and excursions of the real trajectory from this linear drift were extracted, yielding a one-dimensional time series y(t) of length 50 for each segment. For each y(t), the power-spectral density was determined by calculating the square modulus of the Fourier-transformed time series. Then, from each power spectrum the frequency with the largest amplitude, f, was selected and considered for the distribution p(f) if the amplitude was larger than a chosen threshold. The threshold was chosen from non-periodic segments y(t) with a broad and featureless power spectrum. By construction, frequencies below $1/(w\Delta t)$ and larger than $1/(2\Delta t)=5$Hz were not accessible. Moreover, the projection of the trypanosomes' helical motion to only two dimensions and the finite length of segments introduce an additional uncertainty of the helical frequency that broadens p(f) beyond the temporal and cell-specific variations in the motion pattern.